



UNIVERSITÀ  
DEGLI STUDI  
FIRENZE

# FLORE

## Repository istituzionale dell'Università degli Studi di Firenze

### **Chemical, Pharmacological, and Structural Characterization of Novel Acrylamide-Derived Modulators of the GABAA Receptor**

Questa è la versione Preprint (Submitted version) della seguente pubblicazione:

*Original Citation:*

Chemical, Pharmacological, and Structural Characterization of Novel Acrylamide-Derived Modulators of the GABAA Receptor / Arias, Hugo R; Pierce, Spencer R; Germann, Allison L; Xu, Sophia Q; Ortells, Marcelo O; Sakamoto, Seiji; Manetti, Dina; Romanelli, Maria Novella; Hamachi, Itaru; Akk, Gustav. - In: MOLECULAR PHARMACOLOGY. - ISSN 0026-895X. - ELETTRONICO. - 104:(2023), pp. 115-131. [10.1124/molpharm.

*Availability:*

The webpage <https://hdl.handle.net/2158/1344380> of the repository was last updated on 2023-11-08T11:32:04Z

*Published version:*

DOI: 10.1124/molpharm.123.000692

*Terms of use:*

Open Access

La pubblicazione è resa disponibile sotto le norme e i termini della licenza di deposito, secondo quanto stabilito dalla Policy per l'accesso aperto dell'Università degli Studi di Firenze (<https://www.sba.unifi.it/upload/policy-oa-2016-1.pdf>)

*Publisher copyright claim:*

La data sopra indicata si riferisce all'ultimo aggiornamento della scheda del Repository FloRe - The above-mentioned date refers to the last update of the record in the Institutional Repository FloRe

(Article begins on next page)

# **Chemical, Pharmacological, and Structural Characterization of Novel Acrylamide-Derived Modulators of the GABA<sub>A</sub> Receptor**

Hugo R. Arias<sup>a,\*</sup>, Spencer R. Pierce<sup>b</sup>, Allison L. Germann<sup>b</sup>, Sophia Q. Xu<sup>b</sup>, Marcelo O. Ortells<sup>c</sup>, Seiji Sakamoto<sup>d</sup>, Dina Manetti<sup>c</sup>, Maria Novella Romanelli<sup>c</sup>, Itaru Hamachi<sup>d</sup>, and Gustav Akk<sup>b,f</sup>

<sup>a</sup> Department of Pharmacology and Physiology, Oklahoma State University College of Osteopathic Medicine, Tahlequah, Oklahoma, USA

<sup>b</sup> Department of Anesthesiology, Washington University School of Medicine, St. Louis, MO, USA

<sup>c</sup> Facultad de Medicina, Universidad de Morón, Morón, and CONICET, Argentina

<sup>d</sup> Department of Synthetic Chemistry and Biological Chemistry, Graduate School of Engineering, Kyoto University, Kyoto, Japan

<sup>e</sup> Department of Neurosciences, Psychology, Drug Research and Child Health Section of Pharmaceutical and Nutraceutical Sciences, University of Florence, Italy

<sup>f</sup> The Taylor Family Institute for Innovative Psychiatric Research, Washington University School of Medicine, St. Louis, MO, USA

\*Corresponding author: Hugo R. Arias, Department of Pharmacology and Physiology, Oklahoma State University College of Osteopathic Medicine, Tahlequah, Oklahoma, USA

Running title: New modulators of the GABA<sub>A</sub> receptor

Number of manuscript pages: 42

Number of figures: 11

Number of tables: 5

Total word count: 11,636

Number of words in Abstract: 218

Number of words in Introduction: 385

Number of words in Discussion: 851

**Abbreviations:** DM480, (E)-3-(furan-2-yl)-N-(indolin-1-yl)acrylamide; DM489, (E)-3-(furan-2-yl)-1-(indolin-1-yl)prop-2-en-1-one; DM490, (E)-3-(furan-2-yl)-N-methyl-N-(p-tolyl)acrylamide; DM492, (E)-1-(3,4-dihydroquinolin-1(2H)-yl)-3-(furan-2-yl)prop-2-en-1-one; DM495, (E)-1-(3,4-dihydroisoquinolin-2(1H)-yl)-3-(furan-2-yl)prop-2-en-1-one; DM497, (E)-3-(thiophen-2-yl)-N-(p-tolyl)acrylamide; EC<sub>50</sub>, ligand concentration that produces half-maximal activation or potentiation; E<sub>max</sub>, maximal efficacy; etomidate, R(+)-etomidate; GABA<sub>A</sub>R,  $\gamma$ -aminobutyric acid type A receptor; Gzn-OG, gabazine-oregon green; IC<sub>50</sub>, ligand concentration that produces half-maximal inhibition; K<sub>i</sub>, inhibitory constant; nAChR, nicotinic acetylcholine receptor; n<sub>H</sub>, Hill coefficient; PAM, positive allosteric modulator; P<sub>A</sub>, probability of being in the active state; PAM-2, (E)-3-furan-2-yl-N-p-tolyl-acrylamide; PAM-4, (E)-3-furan-2-yl-N-phenylacrylamide; PS, pregnenolone sulfate

## Abstract

Acrylamide-derived compounds have been previously shown to act as modulators of members of the Cys-loop transmitter-gated ion channel family, including the mammalian GABA<sub>A</sub> receptor. Here, we have synthesized and functionally characterized the GABAergic effects of a series of novel compounds (termed "DM compounds") derived from the previously-characterized GABA<sub>A</sub> and the nicotinic  $\alpha 7$  receptor modulator (E)-3-furan-2-yl-*N*-p-tolyl-acrylamide (PAM-2). Fluorescence imaging studies indicated that the DM compounds increase apparent affinity to the transmitter by up to 80-fold in the ternary  $\alpha\beta\gamma$  GABA<sub>A</sub> receptor. Using electrophysiology, we show that the DM compounds, and the structurally-related (E)-3-furan-2-yl-*N*-phenylacrylamide (PAM-4), have concurrent potentiating and inhibitory effects that can be isolated and observed under appropriate recording conditions. The potentiating efficacies of the DM compounds are similar to those of neurosteroids and benzodiazepines ( $\Delta G \sim -1.5$  kcal/mol). Molecular docking, functionally confirmed by site-directed mutagenesis experiments, indicate that receptor potentiation is mediated by interactions with the classic anesthetic binding sites located in the transmembrane domain of the intersubunit interfaces. Inhibition by the DM compounds and PAM-4 was abolished in the receptor containing the  $\alpha 1(V256S)$  mutation, suggestive of similarities in the mechanism of action with that of inhibitory neurosteroids. Functional competition and mutagenesis experiments, however, indicate that the sites mediating inhibition by the DM compounds and PAM-4 differ from those mediating the action of the inhibitory steroid pregnenolone sulfate.

## **Significance Statement**

We have synthesized and characterized the actions of novel acrylamide-derived compounds on the mammalian GABA<sub>A</sub> receptor. We show that the compounds have concurrent potentiating effects mediated by the classic anesthetic binding sites, and inhibitory actions that bear mechanistic resemblance to, but do not share binding sites with, the inhibitory steroid pregnenolone sulfate.

## Introduction

$\gamma$ -Aminobutyric acid type A receptors (GABA<sub>A</sub>Rs) are members of the pentameric Cys-loop transmitter-gated ion channel family and, together with glycine receptors, are the principal inhibitory receptor-channels in the nervous system. The major physiological function of these receptors is maintaining the balance between inhibitory and excitatory neurotransmission. Dysfunction and dysregulation of GABA<sub>A</sub>Rs can upset the equilibrium between inhibition and excitation in the brain, which may progress into pathological conditions, including depression, anxiety, insomnia, autism, epilepsy, memory impairment, schizophrenia, and addiction (Deidda et al., 2014; Hines et al., 2012; Tang et al., 2021). Accordingly, drugs that modulate GABA<sub>A</sub>R function can be important clinically. There is a long history of the medical use of GABA<sub>A</sub>R potentiators in the treatment of some of these illnesses, including anxiety, epilepsy, insomnia as well as for sedation and anesthesia in clinical procedures (Chua and Chebib, 2017; Saari et al., 2011; Sieghart and Savic, 2018; Sigel and Ernst, 2018; Weir et al., 2017). However, not only the clinical efficacies of some of these medications are borderline but they also can be abused leading to dependence and addiction, making evident the need for new, safer medications.

To develop novel GABAergic agents, a series of acrylamide-based compounds (termed "DM compounds") were synthesized (Fig. 1). The DM compounds are structural analogs of (E)-3-furan-2-yl-*N*-p-tolyl-acrylamide (PAM-2), which potentiates the  $\alpha 7$  nicotinic receptor (Arias et al., 2020) and several subtypes of the GABA<sub>A</sub>R (Arias et al., 2022). Here, we have investigated the GABAergic pharmacological activities of the novel compounds, using fluorescence imaging and two-electrode voltage-clamp electrophysiology. To determine the location and structural components of the binding sites involved in positive and negative modulatory activity of DM compounds, site-directed mutagenesis, molecular docking and molecular dynamics (MDs) studies were performed on the  $\alpha 1\beta 2\gamma 2$ L GABA<sub>A</sub>R. The rat  $\alpha 1\beta 2\gamma 2$  GABA<sub>A</sub>R model was constructed using the 3D structure of the human  $\alpha 1\beta 2\gamma 2$  GABA<sub>A</sub>R (Kim et al., 2020). The study is exploratory by nature. The findings are reported according to the guidelines detailed in (Michel et al., 2020).

The main findings of the study are that the tested DM compounds and the structurally-related (E)-3-furan-2-yl-*N*-phenylacrylamide (PAM-4) both potentiate and inhibit the GABA<sub>A</sub>R at high micromolar concentrations. Receptor potentiation is mediated by the compounds acting at the classic anesthetic binding sites in the intersubunit interfaces whereas mutations to the second transmembrane domain strongly reduce inhibition by PAM-4.



## Materials and Methods

### Drugs

R(+)-Etomidate (etomidate) was purchased from Toronto Research Chemicals Inc. (North York, Ontario, Canada). The salts used in buffers, HEPES, GABA, propofol, DMEM high glucose, fetal bovine serum, and 0.01% poly-L-Lys solution (70-150 kDa) were purchased from Sigma-Aldrich (St. Louis, MO, USA). Pregnenolone sulfate was purchased from Bio-Techne Corp. (Minneapolis, MN, USA) and Sigma-Aldrich. Phenobarbital was obtained from J.T. Baker Chemical Co (Phillipsburg, NJ, USA). Lipofectamine 2000, Opti-MEM, and trypsin-EDTA were obtained from Thermo Fischer Scientific (Waltham, MA, USA). (E)-3-(furan-2-yl)acrylic acid, (E)-3-(2-thienyl)acrylic acid, 1-hydroxybenzotriazole hydrate (HOBt), *p*-toluidine, tetrahydroquinoline, tetrahydroisoquinoline and 1-aminoindoline hydrochloride were obtained from Sigma-Aldrich SRL (Milan, Italy). *N*-(3-dimethylaminopropyl)-*N'*-ethylcarbodiimide hydrochloride (EDC), triethylamine, sodium hydride and iodomethane were purchased from Fluorochem (Glossop, UK). Gabazine-oregon green (Gzn-OG) was synthesized as described previously (Sakamoto et al., 2019).

### Chemical synthesis of DM compounds

The method previously described for the synthesis of PAM-2 and DM489 (Arias et al., 2020) was applied for the synthesis of novel compounds and PAM-4 (Fig. 1). The procedure is given for the preparation of DM497. (E)-3-(2-thienyl)acrylic acid (1.0 mmol) was dissolved in anhydrous dichloromethane (5 mL) and the solution cooled to 0 °C. Then, triethylamine (2.0 mmol) and *p*-toluidine (1.0 mmol) were added, and the mixture was stirred for 1 h at 0 °C. Next, 1-hydroxybenzotriazole hydrate (HOBt) (2.0 mmol) and *N*-(3-dimethylaminopropyl)-*N'*-ethylcarbodiimide hydrochloride (EDC) (2.0 mmol) were added, and the mixture stirred for 18 h at room temperature (RT). The mixture was then treated with dichloromethane (15 mL), and the organic layer washed with 6 N HCl (2 x 5 mL). After drying over sodium sulphate, the solvent was removed under reduced pressure, and the residue purified by silica gel flash chromatography

[dichloromethane:methanol; 99:1 (v/v)], obtaining DM497 in 84% yield.

The same method was applied to obtain DM492 [(E)-1-(3,4-dihydroquinolin-1(2H)-yl)-3-(furan-2-yl)prop-2-en-1-one], DM495 [(E)-1-(3,4-dihydroisoquinolin-2(1H)-yl)-3-(furan-2-yl)prop-2-en-1-one], and DM480 [(E)-3-(furan-2-yl)-N-(indolin-1-yl)acrylamide], by coupling (E)-3-(2-furanyl)acrylic acid with tetrahydroquinoline, tetrahydroisoquinoline, or 1-aminoindoline hydrochloride, respectively. Silica gel flash chromatography was performed using hexane:ethyl acetate (8:2, v/v) for the purification of DM492 and DM495, which were obtained in 16% and 18% yield, respectively. The eluent for the purification of DM480 was dichloromethane:methanol:NH<sub>4</sub>OH (99:1:0.1, by vol), and the compound was obtained in 67% yield.

For the synthesis of DM490 [(E)-3-(furan-2-yl)-N-methyl-N-(p-tolyl)acrylamide], PAM-2 was prepared as reported in Arias et al. (2020) and used as starting material. Briefly, 1.0 mmol PAM-2 was dissolved in anhydrous tetrahydrofuran (5 mL) and the solution cooled to 0 °C. Sodium hydride (2.0 mmol) was added, and the mixture stirred for 20 min at 0 °C. Then, iodomethane (3.0 mmol) was added and the mixture stirred for 3 h at room temperature. The mixture was next treated with dichloromethane (20 mL), the organic layer washed with water (2 x 5 mL). After drying over sodium sulphate, the solvent was removed under reduced pressure, and the residue purified by flash silica gel chromatography, with 50% yield.

### **Molecular descriptors for DM compounds**

The molecular descriptors molecular volume, numbers of hydrogen bond donors and acceptors, lipophilicity (LogP) and estimates of brain penetration (LogBB) of the DM compounds were calculated using the Biovia Discovery Studio software (Dassault Systèmes Co., MA, USA). The results are provided for reference purposes in Table 1.

### **Fluorescence imaging assays using GABA<sub>A</sub>Rs transiently expressed in HEK293T cells**

Fluorescence imaging assays were conducted on the  $\alpha 1\beta 3\gamma 2L$  GABA<sub>A</sub>R using gabazine-oregon

green (Gzn-OG). Gzn-OG is a GABA<sub>A</sub>R antagonist that becomes fluorescent upon binding to the transmitter binding site (Sakamoto et al., 2019). Mouse  $\alpha 1$ ,  $\beta 3$ , and  $\gamma 2$ L subunits were transiently transfected into HEK293T (CRL-3216, ATCC, Gaithersburg, MD, USA) cells using Lipofectamine 2000 (Thermo Fisher Scientific, Waltham, MA, USA) as described in detail previously (Sakamoto et al., 2019). Contamination for mycoplasma was not routinely tested. HEK293T- $\alpha 1\beta 3\gamma 2$ L cells were incubated with 100 nM Gzn-OG for 5 min at 25 °C, followed by removal of the medium and wash with HEPES-buffered saline. The cells were then titrated with 0.01  $\mu$ M to 30 mM GABA (three concentration points per decade) in the absence or presence of 10-100  $\mu$ M of a DM compound.

Cell fluorescence imaging was performed using confocal laser scanning microscopy (CLSM) with a Carl Zeiss LSM-800 microscope (Carl Zeiss AG, Oberkochen, Germany), equipped with 63 $\times$ , NA = 1.40 oil objective, and GaAsP detector. CLSM images were acquired using an excitation wavelength of 488 nm (0.75 %, Gain 750 V) and setting emission at 520 nm using the Definite Focus module included in LSM-800. Cell fluorescence was determined by enclosing the regions of interest. Non-specific fluorescence was determined at 30 mM GABA that was assumed to fully displace Gzn-OG. The values of fluorescence are given as mean  $\pm$  S.E.M., from the specified number of cells (in all cases,  $\geq 12$ ).

Apparent IC<sub>50</sub>s for GABA were estimated from non-linear regression fitting of the pooled F/F<sub>0</sub> ratios (KaleidaGraph 4.5, Synergy Software, Reading, PA, USA) using the following logistic equation:

$$F/F_0 = \frac{1}{1 + \left( \frac{IC_{50}}{[GABA]} \right)^{n_H}} \quad (1)$$

where F<sub>0</sub> and F are fluorescence intensity in the absence and presence, respectively, of GABA, [GABA] is the concentration of GABA, IC<sub>50</sub> is the concentration of GABA that produces half-maximal inhibition of fluorescence, and n<sub>H</sub> describes the slope of the curve. The fitted IC<sub>50</sub>s (best-fit

parameters  $\pm$  standard error of the fit) were transformed to apparent  $K_{d,GABA}$  (equilibrium dissociation constant) using the Cheng-Prusoff equation (Cheng and Prusoff, 1973):

$$K_{d,GABA} = \frac{IC_{50}}{1 + \frac{[Gzn-OG]}{K_{d,Gzn-OG}}} \quad (2)$$

where [Gzn-OG] is the initial concentration of Gzn-OG (100 nM) and  $K_{d,Gzn-OG}$  (55 nM) is the  $K_d$  for Gzn-OG (Sakamoto et al., 2019). The reported uncertainties for  $K_{d,GABA}$  reflect error of the fit propagated through Eq. (2).

### Pharmacological activity of novel DM compounds at $\alpha 1\beta 2\gamma 2L$ and $\alpha 1\beta 3\gamma 2L$ GABA<sub>A</sub>R subtypes

Rat  $\alpha 1\beta 2\gamma 2L$  or human  $\alpha 1\beta 3\gamma 2L$  GABA<sub>A</sub>Rs were expressed in *Xenopus laevis* oocytes as previously described (Pierce et al., 2022; Shin et al., 2017). The oocytes were purchased as quarter ovaries from Xenopus 1 (Dexter, MI, USA). The cDNAs for the  $\alpha 1$ ,  $\beta 2$ ,  $\beta 3$ , and  $\gamma 2L$  in the pcDNA3 vector were linearized with XbaI (NEB Labs, Ipswich, MA, USA). The cRNAs were synthesized from linearized cDNA using mMessage mMachine (Ambion, Austin, TX, USA). The oocytes were injected with a total of 3.5 ng of cRNA per oocyte in the cRNA ratio of 1:1:5 ( $\alpha$ : $\beta$ : $\gamma$ ). The  $\gamma 2L$  subunit cRNA was used in excess to enhance incorporation of the  $\gamma 2L$  subunit and to minimize the expression of binary  $\alpha 1\beta 2$  or  $\alpha 1\beta 3$  receptors. Following injection, the oocytes were incubated in ND96 buffer (96 mM NaCl, 2 mM KCl, 1.8 mM CaCl<sub>2</sub>, 1 mM MgCl<sub>2</sub>, 5 mM HEPES; pH 7.4), supplemented with 2.5 mM sodium pyruvate, 50  $\mu$ g/mL gentamycin, 100 U/mL penicillin and, 100  $\mu$ g/mL streptomycin, at 15 °C for 1-2 days prior to conducting electrophysiological recordings.

The electrophysiological recordings were done using standard two-electrode voltage clamp at room temperature. The oocytes were clamped at -60 mV. The chamber (RC-1Z, Warner Instruments, Hamden, CT, USA) was perfused with ND96 at 4-6 mL/min. Solutions were gravity-applied from 30-ml glass syringes with glass luer slips via Teflon tubing and switched manually. Voltage-recording and current-injecting electrodes were pulled from G120F-4 borosilicate glass (Warner Instruments). When filled with 3 M KCl the pipette resistances were 0.3-1 M $\Omega$ . The current

responses were amplified with an Axoclamp 900A (Molecular Devices, San Jose, CA, USA) or OC-725C amplifier (Warner Instruments), digitized with a Digidata 1320 or 1200 series digitizer (Molecular Devices), and stored on PC hard drive using pClamp (Molecular Devices). The current traces were analyzed using Clampfit (Molecular Devices) to determine current amplitude.

The effects of the modulators were estimated by comparing amplitudes of responses to GABA in the presence and absence of a modulator. The experiments were done as "continuous applications" where a cell is first exposed to GABA for up to several minutes, followed without washout by exposure to GABA + modulator, or as standard, separate applications where exposures to GABA and GABA + modulator are separated by washouts (>2 min) in bath solution. In potentiation concentration-response experiments, each cell was exposed to the full range of potentiator concentrations. In inhibition measurements, each cell was exposed to a single application of a single concentration of the inhibitor, and the concentration-response relationship was determined from pooled data. Concentration-response relationships were analyzed by fitting the curves to the Hill equation. Mechanistic analysis of modulatory effects of the DM compounds was done in the framework of the two-state (Resting-Active) concerted transition model as described in detail previously (Akk et al., 2018; Steinbach and Akk, 2019). The peak responses to GABA or GABA + modulator were converted to units of probability of being in the active state ( $P_A$  units) by normalizing the responses to the peak response to 1 mM GABA + 50  $\mu$ M propofol in the same cell (Eaton et al., 2016). The latter was considered to have a peak  $P_A$  indistinguishable from 1 (Shin et al., 2017). The  $P_A$  data were fitted to the state function:

$$P_A = \frac{1}{1 + L^* \left[ \frac{1 + [\text{modulator}] / K_{R,\text{modulator}}}{1 + [\text{modulator}] / (K_{R,\text{modulator}} c_{\text{modulator}})} \right]^{N_{\text{modulator}}}} \quad (3)$$

where  $L^*$  expresses the  $P_A$  of activity in the presence of low GABA alone and is calculated as  $(1 - P_{A,\text{GABA}}) / P_{A,\text{GABA}}$ .  $K_R$  is the equilibrium dissociation constant for the modulator in the resting receptor,  $c$  is the ratio of the equilibrium dissociation constant in the active receptor to  $K_R$ ,  $[\text{modulator}]$  is the

concentration of a DM compound, and  $N$  is the number of DM binding sites (constrained to two).

Curve-fitting was done using Origin 2020 (OriginLab Corp, Northampton, MA, USA).

The extent of modulation,  $K_R$ , and  $c$  values are reported as mean  $\pm$  S.D. Sensitivity to potentiator ( $EC_{50}$ ) is reported as geometric mean with 95% confidence interval. Sensitivity to inhibitor ( $IC_{50}$ ) was estimated from pooled data and is reported as best-fit parameter  $\pm$  standard error of the fit.

### **Molecular docking and molecular dynamics studies on the GABA<sub>A</sub>R model**

The molecular model of the rat  $\alpha 1\beta 2\gamma 2$  GABA<sub>A</sub>R was constructed using the structure of the human  $\alpha 1\beta 2\gamma 2$  GABA<sub>A</sub>R [PDB: 6X3T; (Kim et al., 2020) ] as a homolog template *via* the Prime module of the Schrödinger Suite Release 2020-3 (Schrödinger, LLC, New York, NY, USA). For molecular docking studies, the structures of the DM compounds and PAM-4 were prepared using 2D Sketcher and LigPrep within Schrödinger Maestro (Maestro Version 12.5.139) and evaluated for their ionization states at pH 7.4. Each ligand was docked to different subunit interfaces (i.e.,  $\beta/\alpha$ ,  $\alpha/\beta$ ,  $\alpha/\gamma$ , and  $\gamma/\beta$ ) and ion channel of the GABA<sub>A</sub>R model using QuickVina-W (Hassan et al., 2017), with the exhaustiveness parameter set to 300. Ten docking runs were performed under the same conditions, each producing twenty poses. The poses with more negative theoretical binding energy (TBE) values, obtained as described below, indicating higher theoretical binding affinities, were kept.

To maximize the conformer searching, the extracellular (ECD) and transmembrane (TMD) domains were also targeted separately. From a total of 200 conformers for each ligand, only those with root mean square deviation (RMSD) values (i.e., inter-molecular conformational changes, and the rotation and translation of the whole molecule) above two, were kept. The accepted conformers were clustered, using the same RMSD values as similarity scores, to define structural binding sites. The core of the QuickVina-W algorithm always implements rotations in every atom-atom rotatable bond of the ligand. However, as we are implementing “blind” docking, receptor residues are kept fixed at their original positions. To implement rotations to the receptor residues, a specific list of

rotatable bonds needs to be given, which is impracticable in blind docking. Usually, this is implemented for docking to well-known binding pockets. To estimate accurate ligand TBEs, the rescoring protocol MM-GBSA (Wang et al., 2019) in Schrodinger Prime (Schrödinger, 2020) was used instead scoring functions as those found in QuickVina-W. This procedure allowed us to select, from the initial 600 conformers, the conformer with the best theoretical binding affinity (i.e., more negative TBE values), at each binding site. MM-GBSA energies, are thus used to rank the hundreds of initial poses for each compound at every docking site, with more accurate values than those by the docking method “scores”, however, they cannot be translated directly to  $K_D$  values. For this aim, i.e. to obtain “absolute” binding energies, more sophisticated and time consuming approaches are needed, such as alchemical methods (Williams-Noonan et al., 2018), but this is impracticable for the number of poses we need to analyze.

The final selected docked conformers were further analyzed using molecular dynamics (MDs) to determine their stability and behavior within the binding site. Here, the ligands and the whole receptor are free to move during the MD. First, membrane building (dipalmitoylphosphatidylcholine and cholesterol), complex solvation and ionization were carried out using the CHARMM-GUI membrane builder input generator (Wu et al., 2014). The system, consisting of a hexagonal box of  $X=92\text{\AA}$ ,  $Y=92\text{\AA}$ , and  $Z=120\text{\AA}$  dimension, 70 dipalmitoylphosphatidylcholine molecules, and 9 cholesterol molecules in each leaflet, was neutralized with 0.15 M KCl. To determine the stability of the selected poses within their predicted docking sites, MD simulations of 100 ns were performed using the program NAMD, CHARMM force field (Huang et al., 2017), and the CHARMM-GUI NAMD input generator. Energy minimization of the complexes was first performed, followed by several equilibration MDs (a total of 12 ns for the equilibration), where decreasing harmonic restraints were applied to the backbone atoms. Finally, 100 ns production MDs were performed with no restrictions, using a canonical NPT ensemble and a Nose-Hoover Langevin piston pressure control, at 298 K. The MD protocol includes a timestep size of 2 fs, with 20 timesteps per cycle (the number of timesteps between atom reassignments). The cutoff value for non-bond energy evaluation

was 10 Å. A distance of 8 Å for the switching function was used. Pairs of bonded atoms excluded from non-bonded interaction calculations was determined to 1-4, that is, no non-bonded interactions were calculated for lists of 4 consecutive bonded atoms. RMSD values for each ligand were extracted every 10-ps from the MD simulations using the VMD (Humphrey et al., 1996) RMSD Visualizer Tool plugin. Poses with RMSD variance (VAR) < 0.2 during the last third of the MD were considered stable, those with RMSD VAR values between 0.2 and 2 were considered nearly stable, and those with RMSD VAR values >2 were considered unstable. We also considered stable ligand-residue interactions that maintain, for at least 99% of the MD simulation, a distance  $\leq 5$  Å between the closest atoms and a distance  $\leq 7$  Å between the mass centers. MD simulations were performed using the PETE supercomputer at the High Performance Computing Center (Oklahoma State University-Center for Health Sciences, Tulsa, OK).



## Results

### Chemical synthesis and chemical characterization of the novel DM compounds

The method previously described for the synthesis of PAM-2 and DM489 (Arias et al., 2020) was applied to the synthesis of novel compounds. For DM497, (E)-3-(2-thienyl)acrylic acid was coupled with p-toluidine, using EDC and HOBt as coupling reagents. For DM492, DM495 and DM480, and PAM-4, (E)-3-(2-furanyl)acrylic acid was coupled with tetrahydroquinoline, tetrahydroisoquinoline, 1-aminoindoline hydrochloride or aniline, using EDC and HOBt as coupling reagents. (Fig. 1A). For the synthesis of DM490, PAM-2, used as a starting point, was deprotonated with sodium hydride and methylated using iodomethane (Fig. 1B). All compounds are >95% pure as determined by HPLC/diode-array detection (DAD) analysis. The chemical characteristics of PAM-2, DM489, and PAM-4 have been reported earlier (Arias et al., 2020; Arias et al., 2011). The chemical characterization of the DM compounds gave the following parameters:

DM497 [(E)-3-(thiophen-2-yl)-N-(p-tolyl)acrylamide]:  $^1\text{H}$  NMR ( $\text{CDCl}_3$ , 400 MHz)  $\delta$  2.32 (s, 3H,  $\text{CH}_3$ ), 6.34 (d,  $J = 15.2$  Hz, 1H), 7.04 (dd,  $J = 5.1, 3.7$  Hz, 1H), 7.13 (d,  $J = 8.1$  Hz, 2H), 7.22-7.24 (m, 1H), 7.25 (s, 1H), 7.32 (d,  $J = 5.1$  Hz, 1H), 7.45-7.52 (m, 2H,  $\text{NH} + 1\text{H}$ ), 7.85 (d,  $J = 15.2$  Hz, 1H) ppm.  $^{13}\text{C}$  NMR ( $\text{CDCl}_3$ , 400 MHz)  $\delta$  21.1, 120.53, 125.31, 127.61, 128.02, 129.52, 130.23, 130.42, 134.02, 134.42, 135.71, 140.0, 164.5 ppm. ESI-LC/MS ( $\text{C}_{14}\text{H}_{13}\text{NOS}$ ):  $m/z$  244.3  $[\text{M} + \text{H}]^+$ ; mp 141-142 °C.

DM490 [(E)-3-(furan-2-yl)-N-methyl-N-(p-tolyl)acrylamide]:  $^1\text{H}$  NMR ( $\text{CDCl}_3$ , 400 MHz)  $\delta$  2.39 (s, 3H,  $\text{CH}_3$ ), 3.34 (s, 3H,  $\text{NCH}_3$ ), 6.26 (d,  $J = 15.2$  Hz, 1H), 6.36-6.38 (m, 1H), 6.47 (d,  $J = 3.2$  Hz, 1H), 7.08 (d,  $J = 8.0$  Hz, 2H), 7.24 (d,  $J = 12.8$  Hz, 2H), 7.31 (s, 1H), 7.42 (d,  $J = 15.2$  Hz, 1H) ppm.  $^{13}\text{C}$  NMR ( $\text{CDCl}_3$ , 400 MHz)  $\delta$  20.9, 37.5, 111.9, 113.5, 116.4, 126.9, 128.2, 130.1, 137.3, 140.9, 143.7, 151.6, 165.9 ppm. ESI-LC/MS ( $\text{C}_{15}\text{H}_{15}\text{NO}_2$ ):  $m/z$  242.2  $[\text{M} + \text{H}]^+$ ; mp 108-109 °C.

DM492 [(E)-1-(3,4-dihydroquinolin-1(2H)-yl)-3-(furan-2-yl)prop-2-en-1-one]:  $^1\text{H}$  NMR ( $\text{CDCl}_3$ , 400 MHz)  $\delta$  1.94-2.01 (m, 2H,  $\text{CH}_2$ ), 2.72 (t,  $J = 6.5$  Hz, 2H,  $\text{CH}_2$ ), 3.88 (t,  $J = 6.6$  Hz, 2H,  $\text{CH}_2$ ), 6.40-6.42 (m, 1H), 6.52 (d,  $J = 3.2$  Hz, 1H), 6.74 (d,  $J = 15.2$  Hz, 1H), 7.12-7.37 (m, 4H), 7.37 (s, 1H), 7.50

(d, J = 15.2 Hz, 1H) ppm.  $^{13}\text{C}$  NMR ( $\text{CDCl}_3$ , 400 MHz)  $\delta$  24.10, 26.98, 43.38, 112.14, 113.72, 117.70, 124.99, 125.24, 126.21, 128.41, 128.80, 133.23, 138.57, 144.00, 151.78, 166.02 ppm. ESI-LC/MS ( $\text{C}_{16}\text{H}_{15}\text{NO}_2$ ):  $m/z$  254.3 $[\text{M}+\text{H}]^+$ ; mp 119-120 °C.

DM495 [(E)-1-(3,4-dihydroisoquinolin-2(1H)-yl)-3-(furan-2-yl)prop-2-en-1-one]:  $^1\text{H}$  NMR ( $\text{CDCl}_3$ , 400 MHz)  $\delta$  2.89-2.93 (m, 2H,  $\text{CH}_2$ ), 3.85-3.90 (m, 2H,  $\text{CH}_2$ ), 4.82 (s, 2H,  $\text{CH}_2$ ), 6.42-6.46 (m, 1H), 6.55 (d, J=2.8 Hz, 1H), 6.86 (d, J=15.2 Hz, 1H), 7.18-7.27 (m, 4H), 7.45 (s, 1H), 7.49 (d, J = 15.2 Hz, 1H) ppm.  $^{13}\text{C}$  NMR ( $\text{CDCl}_3$ , 400 MHz)  $\delta$  29.68, 40.30, 42.61, 112.14, 114.03, 114.79, 126.15, 126.84, 128.25, 128.61, 129.29, 142.94, 151.15, 166.10 ppm. ESI-LC/MS ( $\text{C}_{16}\text{H}_{15}\text{NO}_2$ ):  $m/z$  254.3 $[\text{M}+\text{H}]^+$ ; mp 75-78 °C.

DM480 [(E)-3-(furan-2-yl)-N-(indolin-1-yl)acrylamide]:  $^1\text{H}$  NMR ( $\text{CDCl}_3$ , 400 MHz)  $\delta$  3.02-3.12 (m, 3H, CH), 3.61-3.69 (m, 1H, CH), 3.88 (t, J=6.6 Hz, 2H,  $\text{CH}_2$ ), 6.40-6.42 (m, 1H), 6.52 (d, J=3.2 Hz, 1H), 6.74 (d, J=15.2 Hz, 1H), 7.12-7.37 (m, 4H), 7.42 (s, 1H), 7.56 (d, J = 15.2 Hz, 1H) ppm.  $^{13}\text{C}$  NMR ( $\text{CDCl}_3$ , 400 MHz)  $\delta$  24.10, 26.98, 43.38, 112.14, 113.72, 117.70, 124.99, 125.24, 126.21, 128.41, 128.80, 133.23, 138.57, 144.00, 151.78, 166.02 ppm. ESI-LC/MS ( $\text{C}_{15}\text{H}_{14}\text{N}_2\text{O}_2$ ):  $m/z$  254.3 $[\text{M}+\text{H}]^+$ ; mp 125-128 °C.

### **The novel DM compounds increase the apparent affinity of GABA in the $\alpha 1\beta 3\gamma 2\text{L}$ GABA<sub>A</sub>R**

The effect of each DM compound on the apparent binding affinity of GABA at  $\alpha 1\beta 3\gamma 2\text{L}$  GABA<sub>A</sub>Rs was determined by monitoring GABA<sub>A</sub>R-bound Gzn-OG fluorescence at varying concentrations of GABA in the absence and presence of 10-100  $\mu\text{M}$  of each DM compound (Fig. 2). Increasing concentrations of GABA decreased  $\alpha 1\beta 3\gamma 2\text{L}$ -bound Gzn-OG fluorescence, making it nearly undetectable at 1 mM GABA. The inhibition curves were shifted to lower GABA concentrations in the presence of the DM compounds, although the magnitudes of effects differed for individual compounds (Fig. 3). For example, lower Gzn-OG fluorescence was observed in the presence of DM490 compared to DM480, suggesting that the former drug is more efficient in increasing displacement of Gzn-OG by GABA.

Fitting the  $F/F_0$  curves to Eq. 1 yielded  $IC_{50}$  values that were transformed to apparent  $K_{d,GABA}$  using Eq. 2. To assess the variability between GABA titrations, the  $K_{d,GABA}$  were calculated on a daily basis, rendering values between  $13.0 \pm 1.1 \mu M$  and  $19.0 \pm 1.1 \mu M$  (mean  $\pm$  SEM;  $n = 15-22$  cells/titration) (Table 2). In the presence of increasing concentrations of each DM compound, the GABA concentration-response curves were shifted to lower transmitter concentrations (Fig. 3). Considering the  $K_{d,GABA}$  shift between 0 (control) and  $100 \mu M$  DM compound (i.e.,  $K_{d,GABA}/K_{d,GABA,DM}$ ), two populations were discriminated: compounds that induced  $\geq 60$ -fold decrease in  $K_{d,GABA}$  (i.e., DM497, DM490, and DM492), and compounds that produced  $\leq 9$ -fold change (Table 2). Thus, all tested DM compounds increased the apparent binding affinity of GABA, while DM497, DM490, and DM492 produced the largest effects. DM480 was largely ineffective (Fig. 3).

We also assessed whether the most potent DM compounds directly affect the interaction of Gzn-OG with the orthosteric site at  $GABA_A$ Rs (Fig. 3G-H). These results indicated that neither DM497 nor DM490 modifies  $\alpha 1\beta 3\gamma 2L$ -bound Gzn-OG. This suggests that the novel compounds allosterically increase the apparent affinity of GABA to the  $\alpha 1\beta 3\gamma 2L$   $GABA_A$ R rather than directly or indirectly modify the interaction of Gzn-OG with orthosteric binding sites.

### **Potentiating effects of the novel DM compounds on $\alpha 1\beta 2\gamma 2L$ and $\alpha 1\beta 3\gamma 2L$ $GABA_A$ Rs**

Next, we employed two-electrode voltage-clamp electrophysiology to assess the activity of the novel DM compounds and PAM-4 on the synaptic-type  $\alpha 1\beta 2\gamma 2L$   $GABA_A$ R. To better align the electrophysiological data to fluorescence measurements, selected experiments were additionally conducted on the  $\alpha 1\beta 3\gamma 2L$  subtype. The overall findings are that DM489, DM490, DM492, DM495 and DM497 potentiate currents elicited by low GABA and that the modulatory effects of the compounds are similar in  $\alpha 1\beta 2\gamma 2L$  and  $\alpha 1\beta 3\gamma 2L$  receptors. Due to the small effect on fluorescence elicited by DM480, this compound was not studied in electrophysiological recordings.

The concentration-response relationships for DM497, DM492, and DM490 were measured by

coapplying 1-100  $\mu\text{M}$  of each compound with low (3-10  $\mu\text{M}$ ;  $P_A < 0.20$ ) GABA. Fitting the concentration-response curves to the Hill equation gave the  $\text{EC}_{50}$  values (geometric means with 95% confidence intervals) of 32  $\mu\text{M}$  [20 to 50  $\mu\text{M}$ ] for DM497, 15  $\mu\text{M}$  [11 to 19  $\mu\text{M}$ ] for DM492, and 12  $\mu\text{M}$  [10 to 15  $\mu\text{M}$ ] for DM490. Sample current traces and the concentration-response relationships are shown in Figure 4 and summarized in Table 3. DM489 and DM495 were relatively weak modulators, accordingly full concentration-response relationships were not measured. Both compounds were without effect on low-GABA currents at 10  $\mu\text{M}$ . At 50  $\mu\text{M}$ , DM489 and DM495 potentiated the responses to GABA to  $144 \pm 9\%$  ( $n = 5$ ) or  $189 \pm 53\%$  ( $n = 5$ ) of control, respectively.

The potentiating effects of DM497, DM492 and DM490 were further analyzed in the framework of the two-state (Resting-Active) co-agonist model (Steinbach and Akk, 2019). Fitting the concentration-response data to Eq. 3 yielded  $K_R$  (the equilibrium dissociation constant for the modulator in the resting receptor) values of  $50 \pm 33$   $\mu\text{M}$ ,  $19 \pm 7$   $\mu\text{M}$  and  $22 \pm 3$   $\mu\text{M}$ , and  $c$  (the ratio of the equilibrium dissociation constant in the active receptor to  $K_R$ ) values of  $0.391 \pm 0.157$ ,  $0.409 \pm 0.157$  and  $0.224 \pm 0.048$  for DM497, DM492 and DM490, respectively (Table 3). The calculated free energy change [ $\Delta G = NRT \ln(c)$ ] to stabilize the active state ranges from -1.13 kcal/mol (DM492) to -1.79 kcal/mol (DM490) (Table 3). To put this in wider perspective, the  $\Delta G$  values are similar to those of the neurosteroid allopregnanolone and the benzodiazepine diazepam (Cao et al., 2018; Shin et al., 2019), and the previously-reported structural analog of the DM compounds, PAM-2 (Arias et al., 2022).

To better link electrophysiology to fluorescence data, additional experiments were conducted on the  $\alpha 1\beta 3\gamma 2\text{L}$  receptor. The receptor was activated by a low concentration (1-2  $\mu\text{M}$ ;  $< \text{EC}_{15}$ ) of GABA, and the modulatory effects of each compound measured. The DM compounds were tested at concentrations (50  $\mu\text{M}$ ) that produced a near-saturating effect in the  $\alpha 1\beta 2\gamma 2\text{L}$  receptor. The main finding is that the magnitudes of potentiating effects of the DM compounds are statistically (t-test; Excel, Microsoft, Redmond, WA) indistinguishable in  $\alpha 1\beta 2\gamma 2\text{L}$  and  $\alpha 1\beta 3\gamma 2\text{L}$  receptors. The data are

summarized in Figure 5.

### **Inhibitory effects of PAM-4 and the novel DM compounds on the $\alpha 1\beta 2\gamma 2L$ GABA<sub>A</sub>R**

PAM-4 inhibited responses to low GABA. Coapplication of 1-500  $\mu$ M PAM-4 reduced the responses to 2-5  $\mu$ M GABA ( $P_A < 0.10$ ) to ~50% of control, with the  $IC_{50}$  at  $54 \pm 7$   $\mu$ M (best-fit parameter  $\pm$  standard error of the fit of pooled data,  $n = 5-11$  oocytes per concentration). Sample current traces and the concentration-response curve are given in Figure 6.

To determine if inhibition by PAM-4 and potentiation by DM497 is mediated by same or distinct sites, we measured and analyzed potentiation of GABA-activated receptors by DM497 in the presence of a fixed concentration of PAM-4. We reasoned that if PAM-4 acts independently of DM497 then its effect manifests as reduced current response both in the absence and presence of DM497. In this model, the fitted affinity and efficacy parameters describing receptor potentiation by DM497 are expected to be indistinguishable from those estimated in the absence of PAM-4. In contrast, if PAM-4 inhibits and DM497 potentiates the receptor through the same set of binding sites then the inhibitory effect of PAM-4 is expected to manifest as reduced apparent affinity of DM497 (increased  $K_{R,DM497}$ ) but enhanced apparent efficacy (reduced apparent  $c_{DM497}$ ) because at high concentrations DM497 outcompetes PAM-4 and the extent of potentiation reaches the control level.

We recorded GABA-elicited currents in the presence of 1-100  $\mu$ M DM497 coapplied with 50  $\mu$ M or 200  $\mu$ M PAM-4 (Fig. 6B). Coapplication of 50  $\mu$ M PAM-4 reduced the  $P_A$  of the response to 2  $\mu$ M GABA from  $0.057 \pm 0.011$  to  $0.041 \pm 0.011$  ( $n = 6$ ). Exposure to 100  $\mu$ M DM497 enhanced the response to GABA + PAM-4 to  $0.122 \pm 0.03$ . The  $EC_{50}$  of the potentiation curve was 26  $\mu$ M [23 to 30  $\mu$ M] (Fig. 6C), which is not significantly different from the  $EC_{50}$  for potentiation by DM497 in the absence of PAM-4 (32  $\mu$ M, see above). Fitting of the potentiation curve to Eq. 3 yielded a  $K_{R,DM497}$  of  $29 \pm 9$   $\mu$ M and a  $c_{DM497}$  of  $0.454 \pm 0.031$ . Neither value is significantly different from the estimates in the absence of PAM-4. In the presence of 200  $\mu$ M PAM-4, the  $EC_{50}$  of the DM497 potentiation curve was 28  $\mu$ M [24 to 33  $\mu$ M], and the fitted  $K_{R,DM497}$  and  $c_{DM497}$   $43 \pm 21$   $\mu$ M and

$0.618 \pm 0.036$ , respectively. The  $EC_{50}$  and  $K_{R,DM497}$  estimates are not different from those in the absence of PAM-4, but  $c_{DM497}$  is significantly ( $P < 0.05$ ) higher than that in the absence of PAM-4. The reason for higher  $c_{DM497}$  (i.e., reduced apparent efficacy) in the presence of 200  $\mu$ M PAM-4 is unclear, however we note that such an effect is the opposite to what is expected if PAM-4 and DM497 bind to overlapping sites. In sum, we infer that GABA<sub>A</sub>R inhibition by PAM-4 and potentiation by DM497 are mediated by distinct sites.

State-dependence of inhibition and distinct mechanisms of inhibition manifest in dissimilar sensitivity to inhibitor at different levels of activity (Germann et al., 2022). To gain insight into the mechanism of inhibition by PAM-4, we compared the magnitude of inhibition at low (2-5  $\mu$ M; peak  $P_A=0.1$ ) and high (1 mM; peak  $P_A=0.9$ ) GABA. Application of 50 or 200  $\mu$ M PAM-4 reduced the response to low GABA to  $81 \pm 8\%$  ( $n = 5$ ) or  $48 \pm 16\%$  ( $n = 11$ ) of control, and the response to high GABA to  $84 \pm 7\%$  ( $n = 5$ ) or  $58 \pm 11\%$  ( $n = 5$ ) of control, respectively. The magnitudes of effects are statistically indistinguishable. We infer that PAM-4 similarly inhibits resting, active, and desensitized receptors.

### **The $\alpha 1(V256S)$ mutation abolishes inhibition by PAM-4 and the novel DM compounds**

Under recording conditions where potentiation dominates, i.e., at low fractional activities, small inhibitory effects can be masked by a separate, stronger potentiating effect. To test if the DM compounds can inhibit the GABA<sub>A</sub>R, we measured the effect of each DM compound (DM490, DM497, DM492, DM489, DM495) on steady-state current elicited by 1 mM GABA. At this concentration of agonist, potentiating effects of a drug are masked due to the high  $P_A$  (0.9) of the current response (Shin et al., 2017; Szabo et al., 2019). The main finding is that all compounds inhibited responses to GABA. The effects among the compounds, applied at 50  $\mu$ M, were relatively similar with the magnitude of inhibition ranging from  $33 \pm 7\%$  ( $n = 5$ ; DM489) to  $46 \pm 15\%$  ( $n = 5$ ; DM495). The data are summarized in Figure 7A-B.

The  $\alpha 1(V256S)$  mutation (2' residue in TM2) drastically reduces the actions of inhibitory

neurosteroids and analogs (Akk et al., 2001; Li et al., 2006b; Wang et al., 2002). To probe if receptor inhibition by PAM-4 and the DM compounds involves the mechanism utilized by inhibitory neurosteroids, we measured inhibition of the  $\alpha 1(V256S)\beta 2\gamma 2L$  GABA<sub>A</sub>R by PAM-4 and the DM compounds. The receptors were initially exposed to 1 mM GABA ( $P_{A,peak} = 0.87 \pm 0.12$ ,  $n = 28$ ). At appr. 4-min time point, the solution was switched to GABA + 50  $\mu$ M modulator, followed by wash in GABA. The main finding is that in the mutant receptor, coapplication of a modulator had minimal (<2%) inhibitory effect on the response to GABA. The data are summarized in Figure 7A-B.

In control experiments, we tested DM-mediated potentiation of the  $\alpha 1(V256S)\beta 2\gamma 2L$  receptor activated by low (0.05  $\mu$ M;  $P_A = 0.07 \pm 0.05$ ,  $n = 26$ ) GABA. The mutation did not reduce the potentiating effects of the DM compounds (Fig. 7C-D). Interestingly, we observed a small ( $109 \pm 2\%$  of control;  $n = 5$ ) but statistically significant ( $P < 0.001$  vs. no effect, paired t-test; Excel, Microsoft) potentiating effect in the presence of 100  $\mu$ M PAM-4. We infer that the  $\alpha 1(V256S)$  mutation selectively reduces the inhibitory effects of PAM-4 and the DM compounds. From these data, we propose that all tested compounds have potentiating and inhibitory actions on the  $\alpha 1\beta 2\gamma 2L$  GABA<sub>A</sub>R while the magnitude and direction of the observed effect depend on recording conditions (low vs. high GABA, presence of the V256S mutation) that may selectively mask potentiation or inhibition.

### **DM490 and DM497 stably dock to the anesthetic sites, whereas PAM-4 also docks to the ion channel lumen of the $\alpha 1\beta 2\gamma 2$ model**

Initial molecular docking results indicated that DM490, DM497, and PAM-4 interact with the classic anesthetic binding sites located at the intersubunit interfaces of the  $\alpha 1\beta 2\gamma 2$  model (Fig. 8A), with binding energies in the -30 to -40 kcal/mol range (Table 4). DM497 and PAM-4 also interacted with the homologous site at the  $\alpha +/\gamma -$  interface, i.e., at the interface formed by the "+" side of the  $\alpha$  subunit and the "-" side of the  $\gamma$  subunit (Fig. 8A, middle panel) and ion channel (Fig. 8A, right panel), respectively. To determine ligand stability in each docking site, RMSD variance (VAR)

values during the last third of the MD simulations (100 ns) were calculated. Table 4 shows the theoretical binding energies (TBE) of the poses, along with their RMSD and RMSD VAR values, and the stability classification based on the latter (defined as “stable”, “near stable”, and “unstable”), as explained in Methods. The residue interactions of the stable poses are shown in Table 5. The docking of DM490, DM497, and PAM-4 at the  $\beta^+/\alpha^-$  site were considered stable. Each ligand made contact with practically the same residues:  $\beta$ -TM2 (M261, T262, and N265) and  $\beta$ -TM3 residues (L285, M286, F289, and V290) (Table 5). In particular, DM490 established a  $\pi$ - $\pi$  interaction with F289. At the  $\alpha^+/\beta^-$  site, only DM490 remained stable (Table 4), making contacts with  $\alpha$ -TM2 (T267 and S270),  $\alpha$ -TM3 (A283, D287, W288, I290, A291, and Y294), and  $\beta$ -TM1 residues (L223, M227, P228, and L231) (Table 5). DM490 also established a  $\pi$ - $\pi$  interaction with  $\alpha$ Y294. Figures 9A-B show the molecular interactions for DM490 at the respective  $\beta^+/\alpha^-$  and  $\alpha^+/\beta^-$  site.

DM497 was the only compound forming stable interactions with the anesthetic  $\gamma^+/\beta^-$  and  $\alpha^+/\gamma^-$  sites. In the  $\gamma^+/\beta^-$  site, DM497 made contact with  $\gamma$ -TM2 (T277, S280; M3 S301, F304, I305, and F308) and  $\beta$ -TM1 residues (L223, Q224, M227, P228, and L231) (Table 5). In the  $\alpha^+/\gamma^-$  site, DM497 interacted with  $\alpha$ -TM2 (S270, M3 D287, I290, A291, Y294, A295, F298, S299, and I302) and  $\alpha$ -TM1 residues (I238, I242, and L246) (Table 5). Figures 9C-D show the molecular interactions for DM497 at the  $\beta^+/\alpha^-$  and  $\alpha^+/\gamma^-$  sites.

PAM-4 was the only compound showing high stability (VAR = 0.06) in the ion channel site (Table 4), making contact with the  $\alpha$ ,  $\beta$ , and  $\gamma$  subunits (Fig. 9E). PAM-4 directly interacted with the ion channel lumen, more specifically with TM2 rings located at 6' ( $\alpha$ -T261), 9' ( $\gamma$ -L274 and  $\beta$ -L259), and 13' ( $\gamma$ -T278 and  $\beta$ -T263) positions, in addition to other non-luminal residues (Table 5). The differences in the binding interfaces may account for the differences in efficacies among the DM compounds and for the inhibitory activity of PAM-4. Interestingly, although DM490 is the most potent PAM using low GABA concentrations, it inhibits the receptor at high concentrations which we account for by its detection at the site in the channel (Table 4). At this site, DM490 interacts with the  $\alpha$  (M1 P233, T237; M2 T261[6'], L264[9'], T265, M266, T268[13'], and L269) and  $\beta$  (V258,



L259[9'], T260, M261, T262, and T263[13']) residues.

### Functional insights into potentiating sites

A combination of agonists acting independently through distinct sites generates a larger potentiating effect and response than a combination of agonists that acts through same or overlapping sites (Shin et al., 2019). Molecular docking studies suggested that the DM compounds interact with the anesthetic binding sites in intersubunit interfaces. To confirm this functionally, we compared the potentiating effect of DM490 in receptors activated by GABA and in receptors activated by the anesthetics etomidate or phenobarbital. Etomidate and phenobarbital activate the GABA<sub>A</sub>R by interacting with the anesthetic binding sites in the  $\beta^+/\alpha^-$ , and  $\alpha^+/\beta^-$  and  $\gamma^+/\beta^-$  interfaces, respectively (Chiara et al., 2013; Kim et al., 2020; Li et al., 2006a). We reasoned that if DM490 potentiates the  $\alpha 1\beta 2\gamma 2$ L receptor by interacting with one or more of the anesthetic sites, then its effect on receptors activated by etomidate (or phenobarbital) is smaller than that in receptors activated by GABA. In contrast, if DM490 and etomidate (or phenobarbital) act through non-overlapping sites, and independently, then potentiation is expected to be similar in receptors activated by GABA or the anesthetics. Receptor responses to 5-10  $\mu$ M etomidate ( $P_A = 0.09 \pm 0.05$ ,  $n = 8$ ) were only weakly ( $156 \pm 60\%$  of control) enhanced by 50  $\mu$ M DM490. Coapplication of 50  $\mu$ M DM490 potentiated the response to 1 mM phenobarbital ( $P_A = 0.09 \pm 0.04$ ,  $n = 5$ ) to  $240 \pm 67\%$  of control. For comparison, DM490 potentiated receptors activated by 1  $\mu$ M GABA to  $887 \pm 249\%$  of control (above, Fig. 7D). Sample currents and the summary of potentiation of etomidate- and phenobarbital-activated receptors by DM490 are given in Figure 10A. We propose that GABA<sub>A</sub>R potentiation by DM490 utilizes the classic intersubunit anesthetic binding sites, with a possibly larger functional contribution made by the etomidate-binding  $\beta^+/\alpha^-$  interfaces compared to the phenobarbital-binding  $\alpha^+/\beta^-$  and  $\gamma^+/\beta^-$  interfaces.

Further tests of the involvement of the anesthetic sites in potentiation by the DM compounds were done on receptors containing mutations to one or more intersubunit interfaces. We first tested

the effect of the  $\beta 2(\text{F289A})$  mutation. This residue is in the  $\beta +/\alpha -$  interface where it lines the binding pocket for etomidate and propofol (Chiara et al., 2012; Franks, 2015). Our molecular docking studies place  $\beta 2(\text{F289})$  within 4 Å of the DM490 molecule where it makes a  $\pi$ - $\pi$  interaction with the phenyl group of DM490 (Fig. 8B). In the  $\alpha 1\beta 2(\text{F289A})\gamma 2\text{L}$  receptor, coapplication of 50  $\mu\text{M}$  DM490 potentiated the response to 0.1-0.2  $\mu\text{M}$  GABA ( $P_A = 0.07 \pm 0.05$ ,  $n = 5$ ) to a mere  $114 \pm 6\%$  of control (vs. 887% of control in wild-type; see above). From  $P_{A,50 \mu\text{M DM490}} = 1/(1 + L \times c_{50 \mu\text{M DM490}}^2)$ , we estimate a  $c_{50 \mu\text{M DM490}}$  of  $0.935 \pm 0.027$  and a  $\Delta G$  of  $-0.08 \pm 0.03$  kcal/mol. For comparison, the calculated  $c_{50 \mu\text{M DM490}}$  in the  $\alpha 1\beta 2\gamma 2\text{L}$  receptor is  $0.296 \pm 0.048$  and the  $\Delta G$  is  $-1.45 \pm 0.19$  kcal/mol.

Second, we measured the effect of the  $\alpha 1(\text{Y293C})$  mutation on modulation by DM490. This residue, predicted to make  $\pi$ - $\pi$  interaction with the phenyl group of DM490, is present in the  $\alpha +/\beta -$  interface at the barbiturate binding site (Chiara et al., 2013; Kim et al., 2020) and in the  $\alpha +/\gamma -$  interface, termed the "orphan" interface due to lack of protection by the anesthetics propofol, etomidate or a barbiturate analog in cysteine-modification experiments (Nourmahnad et al., 2016). We note that the rat  $\alpha 1(\text{Y293})$  residue is homologous to the human  $\alpha 1(\text{Y294})$  residue in modelling studies (Fig. 9). In the  $\alpha 1(\text{Y293C})\beta 2\gamma 2\text{L}$  receptor, coapplication of 50  $\mu\text{M}$  DM490 potentiated the response to 0.1-0.2  $\mu\text{M}$  GABA ( $P_A = 0.05 \pm 0.04$ ,  $n = 5$ ) to  $891 \pm 353\%$  of control (Fig. 10C). The magnitude of potentiation was indistinguishable from potentiation observed in the  $\alpha 1\beta 2\gamma 2\text{L}$  receptor. The calculated  $c_{50 \mu\text{M DM490}}$  is  $0.293 \pm 0.041$  and the  $\Delta G$  is  $-1.46 \pm 0.17$  kcal/mol.

We also measured the effect of  $\gamma 2\text{L}(\text{L246W})$  (10' position after the conserved GYF sequence in TM1). This mutation is present solely in the  $\alpha +/\gamma -$  interface. The  $\alpha 1\beta 2\gamma 2\text{L}(\text{L246W})$  receptor is constitutively active ( $P_{A,\text{constitutive}} = 0.12 \pm 0.04$ ;  $n = 5$ ); accordingly, we measured the direct activating, rather than potentiating, effect of DM490. Application of 50  $\mu\text{M}$  DM490 generated a response with a  $P_A$  of  $0.31 \pm 0.07$  (Fig. 10C). The calculated  $c_{50 \mu\text{M DM490}}$  is  $0.537 \pm 0.032$  and the  $\Delta G$  is  $-0.74 \pm 0.07$  kcal/mol.

In the barbiturate-binding  $\gamma +/\beta -$  interface, we tested the  $\gamma 2\text{L}(\text{F304C})$  mutation. Since the  $\alpha 1\beta 2\gamma 2\text{L}(\text{F304C})$  receptor is constitutively active ( $P_{A,\text{constitutive}} = 0.32 \pm 0.10$ ;  $n = 5$ ), the effect of

DM490 was tested in the absence of GABA. Application of 50  $\mu$ M DM490 increased the  $P_A$  to  $0.46 \pm 0.11$  ( $1.5 \pm 0.2$ -fold potentiation in  $P_A$  units). The calculated  $c_{50 \mu\text{M DM490}}$  and  $\Delta G$  are  $0.736 \pm 0.035$  and  $-0.36 \pm 0.06$  kcal/mol, respectively. The findings on the mutant receptors are summarized in Figure 10D.

In sum, two sets of experiments indicate that the potentiating action of DM490 is mediated by the classic anesthetic binding sites at intersubunit interfaces in the transmembrane domain of the receptor. First, DM490 has a weaker potentiating effect on receptors activated by the anesthetics etomidate or phenobarbital compared to receptors activated by GABA. Second, mutations to the individual intersubunit interfaces, in some cases drastically, reduce the potentiating effect of DM490. We note that with a single exception (the  $\alpha 1(\text{Y293C})$  mutation to the  $\alpha +/\beta -$  interface), the predictions from molecular docking were confirmed in electrophysiological studies.

### Functional insights into inhibitory sites

Sensitivity to the  $\alpha 1(\text{V256S})$  mutation suggests that a mechanism similar to that of inhibitory neurosteroids and analogs (Akk et al., 2001; Li et al., 2006b; Wang et al., 2002) underlies inhibition by PAM-4 and the DM compounds. We emphasize that at this time it is unclear if the  $\alpha 1\text{V256}$  residue is a component of the binding site or a transduction element for inhibitory steroids (Akk et al., 2001). We next investigated whether PAM-4 and the inhibitory steroid pregnenolone sulfate (PS) interact with overlapping binding sites. We recorded the effect of 200  $\mu$ M PAM-4 on steady-state current generated by 1 mM GABA in the presence of 10  $\mu$ M PS. PAM-4 (Fig. 6C) is a lower efficacy inhibitor than PS (Fig. 11A; (Germann et al., 2019; Pierce et al., 2022)). We hypothesized that interaction with overlapping sites would lead to competition with PS-binding and manifest as reduced PS-inhibition in the presence of PAM-4. Application of 10  $\mu$ M PS reduced the steady-state response to 1 mM GABA to  $16 \pm 4\%$  ( $n = 5$ ) of control. Coapplication of 200  $\mu$ M PAM-4 with GABA + PS increased inhibition, reducing the steady-state response to  $11 \pm 3\%$  ( $n = 5$ ) of the control GABA steady-state response (or  $67 \pm 9\%$  of the response to GABA + PS). A sample current

trace is given in Figure 11A. Given increased inhibition when PAM-4 is coapplied with PS, we infer that PAM-4 does not interfere with PS binding to its site.

An analogous experiment was conducted using DM490 as the competing agent. The receptors were activated with 1 mM GABA. Once steady-state response was reached, the cells were exposed to GABA + 10  $\mu$ M PS, followed by an application of GABA + PS + 50  $\mu$ M DM490. In five cells, the application of PS reduced the steady-state response to  $12 \pm 5\%$  of the GABA control response whereas the application of DM490 reduced the response to  $6 \pm 2\%$  of the GABA control response (or  $55 \pm 6\%$  of the GABA + PS response). The effect of 50  $\mu$ M DM490 is similar in the absence (Table 3) and presence of PS. We conclude that PS does not interfere with DM490-elicited inhibition and propose that DM490 and PS bind to distinct sites.

Molecular docking suggested a possible binding site for PAM-4 in the channel lumen where it interacts with residues in the 6', 9', and 13' rings of TM2 (Fig. 9E). To probe the functional involvement of this site, we measured the effects of 200  $\mu$ M PAM-4 on steady-state current elicited by 1 mM GABA in  $\alpha 1\beta 2\gamma 2L(L274C)$  (9' leucine in  $\gamma$ -TM2) and  $\alpha 1\beta 2\gamma 2L(T278C)$  (13' threonine in  $\gamma$ -TM2) receptors. As control, we tested receptor inhibition by 10  $\mu$ M PS. In the  $\alpha 1\beta 2\gamma 2L(L274C)$  receptor, application of PAM-4 reduced the  $P_A$  of the steady-state current from  $0.87 \pm 0.04$  ( $n = 5$ ) to  $0.82 \pm 0.03$  ( $6 \pm 1\%$  inhibition). This should be compared to the  $\sim 50\%$  inhibition in  $\alpha 1\beta 2\gamma 2L$  (Fig. 6A, C). In a control experiment, PS fully abolished receptor activity:  $P_A$  of the steady-state response decreased from  $0.85 \pm 0.07$  ( $n = 5$ ) to  $-0.18 \pm 0.20$ . Sample current traces and data summary are given in Figure 11. In the  $\alpha 1\beta 2\gamma 2L(T278C)$  receptor (Fig. 11C), the  $P_A$  of the steady-state current decreased from  $0.20 \pm 0.08$  ( $n = 5$ ) to  $0.17 \pm 0.06$  ( $11 \pm 11\%$  inhibition) in the presence of PAM-4. In contrast, exposure to PS reduced the  $P_A$  from  $0.18 \pm 0.07$  to  $0.02 \pm 0.01$  ( $90 \pm 2\%$  inhibition). Thus, mutations to selected pore-lining residues in the  $\gamma 2L$  subunit strongly reduce receptor inhibition by PAM-4. The magnitudes of the inhibitory effects of PS in the mutant receptors are similar to those observed in the wild-type ternary  $\alpha\beta\gamma$  receptor (Germann et al., 2019; Pierce et al., 2022) and support the notion that PS and PAM-4 bind to distinct sites. The data are summarized in

Figure 11D.

We conclude that PAM-4 and DM490 inhibit the receptor through interactions with a site that is distinct from that of the inhibitory steroid PS. We have also shown that substitutions of residues in the lumen of the channel (9' and 13' in TM2 of the  $\gamma$ 2L subunit) strongly reduce inhibition by PAM-4 but not by PS.

## Discussion

The objective of this study was to develop and characterize novel acrylamide-derived compounds, based on the structure of the previously-reported GABAergic drug PAM-2 (Arias et al., 2022), as modulators of the GABA<sub>A</sub>R. We show that the newly synthesized compounds, at high micromolar concentrations, concurrently act as allosteric potentiators and inhibitors of the ternary  $\alpha\beta\gamma$  GABA<sub>A</sub>R. The relative magnitudes of the potentiating and inhibitory effects differ among the compounds thereby defining the experimentally observed net functional effect. For example, when tested in the presence of a low concentration of GABA, the strong potentiating effect of DM490 overwhelms its relatively weak inhibitory effect, whereas its much weaker potentiating effect renders PAM-4 a net inhibitory compound. When tested in the presence of saturating GABA, where any observable potentiation is diminished due to the high  $P_A$  of the control response, all compounds produced inhibition.

The free energy changes provided by the most efficacious DM compounds to stabilize the active state (-1.13 to -1.79 kcal/mol for DM492, DM497 and DM490) are similar to those for several neurosteroids, the benzodiazepine diazepam, and the previously-studied acrylamide-based GABA<sub>A</sub>R potentiator PAM-2 (Arias et al., 2022; Cao et al., 2018; Shin et al., 2019). Such compounds do not meaningfully directly activate the wild-type  $\alpha 1\beta 2\gamma 2L$  GABA<sub>A</sub>R (for example, a  $\Delta G$  of -1.4 kcal/mol predicts a  $P_{A,peak}$  of 0.001), but efficaciously potentiate a receptor activated by low concentrations of GABA (a  $\Delta G$  of -1.4 kcal/mol predicts a >5-fold potentiation of an  $EC_{10} / P_A$  0.1 response). DM489 and DM495 were weaker modulators with  $\Delta G$  values at -0.30 to -0.20 kcal/mol, and the potentiating effect of PAM-4 could only be observed when its inhibitory effect was blocked by a mutation.

The potentiating and inhibitory effects of the DM compounds and PAM-4 are mediated by distinct sites. Molecular docking analysis suggested that the DM compounds potentiate the receptor through interactions with the classic anesthetic binding sites in the intersubunit interfaces. In electrophysiological recordings, DM490 had a smaller potentiating effect on receptors activated by the allosteric agonists etomidate and phenobarbital compared to receptors activated by GABA. We

interpret this finding as DM490 sharing binding sites with etomidate and phenobarbital. From the relative effects on etomidate- vs. phenobarbital-activated receptors we propose that the interaction of DM490 with the two  $\beta^+/\alpha^-$  interfaces makes a slightly larger energetic impact than its interaction with the phenobarbital-binding  $\alpha^+/\beta^-$  and  $\gamma^+/\beta^-$  interfaces. We note though that the calculated contributions are not strictly additive. In  $\alpha 1\beta 2\gamma 2L$  receptors activated by GABA alone, in which all anesthetic sites are free to bind the modulator, 50  $\mu M$  DM490 contributes  $-1.45 \pm 0.19$  kcal/mol free energy change towards activation. In etomidate-activated receptors, where the  $\alpha^+/\beta^-$  and  $\gamma^+/\beta^-$  interfaces are presumed vacant, DM490 contributes  $-0.25 \pm 0.23$  kcal/mol, and in phenobarbital-activated receptors, DM490 binding to the  $\beta^+/\alpha^-$  interfaces contributes  $-0.58 \pm 0.18$  kcal/mol. Thus, the loss of potentiation in receptors activated by etomidate or phenobarbital is greater than what is expected in case of independence of sites and energetic additivity. One conceivable explanation is that etomidate and/or phenobarbital interact with interfaces other than those postulated.

Lack of energetic additivity was also observed in experiments on receptors containing mutations to the individual anesthetic binding interfaces. Almost a complete loss of activity ( $\Delta G_{50 \mu M \text{ DM490}} = -0.08 \pm 0.03$  kcal/mol) was observed in the receptor containing the  $\beta 2(F289A)$  mutation in the two  $\beta^+/\alpha^-$  interfaces, suggesting that this interface is the major, nearly sole contributor to activation and potentiation by DM490. On the other hand, mutations to the barbiturate-binding  $\gamma^+/\beta^-$  and the orphan  $\alpha^+/\gamma^-$  interfaces also significantly reduced gating by DM490. The free energy changes supplied by 50  $\mu M$  DM490 were  $-0.36 \pm 0.06$  kcal/mol ( $\Delta\Delta G = 1.09$  kcal/mol vs. wild-type) and  $-0.74 \pm 0.07$  kcal/mol ( $\Delta\Delta G = 0.75$  kcal/mol vs. wild-type) in the  $\alpha 1\beta 2\gamma 2L(F304C)$  and  $\alpha 1\beta 2\gamma 2L(L246W)$  receptors, respectively, overall suggesting strong contributions from interfaces other than  $\beta^+/\alpha^-$ . The most parsimonious explanation is that the anesthetic binding sites in different intersubunit interfaces are allosterically linked as reported previously (Hoyt et al., 2022; Szabo et al., 2019). The putative binding site location is supported by molecular docking and molecular dynamics studies where DM490 stably interacted with the  $\beta^+/\alpha^-$  and  $\alpha^+/\beta^-$  interfaces, whereas DM497 also interacted with the  $\gamma^+/\beta^-$  and  $\alpha^+/\gamma^-$  interfaces.

While receptor inhibition by PAM-4 and the DM compounds shows similarities to the actions of inhibitory neurosteroids, such as sensitivity to the  $\alpha 1$ (V256S) mutation, our functional competition experiments (Fig. 11A) indicate that PAM-4 or DM490, and PS do not share a binding site. This is supported by results on mutant receptors. From molecular docking, we have postulated a binding site for PAM-4 in the channel lumen near the activation gate at the TM2-9'-13' level where mutations to selected residues strongly diminished inhibition by PAM-4 but not by PS (Fig. 11D).

In sum, we report here the chemical synthesis and functional characterization of novel acrylamide-based modulators of the mammalian GABA<sub>A</sub> receptor. The compounds have concurrent potentiating and inhibitory effects with net positive modulatory efficacies reaching that of a number of GABAergic anxiolytics and sedatives. The synthesized compounds have medium to high blood-brain barrier penetration (Table 1), supportive of potential use in clinical practice.



### **Data Availability Statement**

The authors declare that all the data supporting the findings of this study are contained within the paper and its Supplemental Data.

### **Authorship Contributions**

*Participated in research design:* Arias, Ortells, Sakamoto, and Akk.

*Conducted experiments:* Pierce, Germann, Xu, Ortells, and Sakamoto.

*Contributed new reagents or analytic tools:* Manetti, Romanelli, and Hamachi.

*Performed data analysis:* Arias, Pierce, Germann, Xu, Ortells, Sakamoto, and Akk.

*Wrote or contributed to the writing of the manuscript:* Arias, Pierce, Germann, Xu, Ortells, Sakamoto, Manetti, Romanelli, Hamachi, and Akk.

## References

- Akk G, Bracamontes J, and Steinbach JH (2001) Pregnenolone sulfate block of GABA(A) receptors: mechanism and involvement of a residue in the M2 region of the alpha subunit. *J Physiol* **532**: 673-684.
- Akk G, Shin DJ, Germann AL, and Steinbach JH (2018) GABA Type A Receptor Activation in the Allosteric Coagonist Model Framework: Relationship between EC50 and Basal Activity. *Mol Pharmacol* **93**: 90-100.
- Arias HR, Germann AL, Pierce SR, Sakamoto S, Ortells MO, Hamachi I, and Akk G (2022) Modulation of the mammalian GABA<sub>A</sub> receptor by type I and type II positive allosteric modulators of the alpha7 nicotinic acetylcholine receptor. *Br J Pharmacol* **179**: 5323-5337.
- Arias HR, Ghelardini C, Lucarini E, Tae HS, Yousuf A, Marcovich I, Manetti D, Romanelli MN, Elgoyhen AB, Adams DJ, and Di Cesare Mannelli L (2020) (E)-3-Furan-2-yl-N-p-tolyl-acrylamide and its Derivative DM489 Decrease Neuropathic Pain in Mice Predominantly by alpha7 Nicotinic Acetylcholine Receptor Potentiation. *ACS Chem Neurosci* **11**: 3603-3614.
- Arias HR, Gu RX, Feuerbach D, Guo BB, Ye Y, and Wei DQ (2011) Novel positive allosteric modulators of the human alpha7 nicotinic acetylcholine receptor. *Biochemistry* **50**: 5263-5278.
- Bagdas D, Sevdar G, Gul Z, Younis R, Cavun S, Tae HS, Ortells MO, Arias HR, and Gurun MS (2021) (E)-3-furan-2-yl-N-phenylacrylamide (PAM-4) decreases nociception and emotional manifestations of neuropathic pain in mice by alpha7 nicotinic acetylcholine receptor potentiation. *Neurol Res* **43**: 1056-1068.
- Cao LQ, Montana MC, Germann AL, Shin DJ, Chakrabarti S, Mennerick S, Yuede CM, Wozniak DF, Evers AS, and Akk G (2018) Enhanced GABAergic actions resulting from the

- coapplication of the steroid 3 $\alpha$ -hydroxy-5 $\alpha$ -pregnane-11,20-dione (alfaxalone) with propofol or diazepam. *Sci Rep* **8**: 10341.
- Cheng Y and Prusoff WH (1973) Relationship between the inhibition constant (K<sub>1</sub>) and the concentration of inhibitor which causes 50 per cent inhibition (I<sub>50</sub>) of an enzymatic reaction. *Biochem Pharmacol* **22**: 3099-3108.
- Chiara DC, Dostalova Z, Jayakar SS, Zhou X, Miller KW, and Cohen JB (2012) Mapping general anesthetic binding site(s) in human  $\alpha 1\beta 3\gamma 2$  gamma-aminobutyric acid type A receptors with [(3)H]TDBzl-etomidate, a photoreactive etomidate analogue. *Biochemistry* **51**: 836-847.
- Chiara DC, Jayakar SS, Zhou X, Zhang X, Savechenkov PY, Bruzik KS, Miller KW, and Cohen JB (2013) Specificity of intersubunit general anesthetic-binding sites in the transmembrane domain of the human  $\alpha 1\beta 3\gamma 2$   $\gamma$ -aminobutyric acid type A (GABA<sub>A</sub>) receptor. *J Biol Chem* **288**: 19343-19357.
- Chua HC and Chebib M (2017) GABAA Receptors and the Diversity in their Structure and Pharmacology. *Adv Pharmacol* **79**: 1-34.
- Deidda G, Bozarth IF, and Cancedda L (2014) Modulation of GABAergic transmission in development and neurodevelopmental disorders: investigating physiology and pathology to gain therapeutic perspectives. *Front Cell Neurosci* **8**: 119.
- Eaton MM, Germann AL, Arora R, Cao LQ, Gao X, Shin DJ, Wu A, Chiara DC, Cohen JB, Steinbach JH, Evers AS, and Akk G (2016) Multiple Non-Equivalent Interfaces Mediate Direct Activation of GABAA Receptors by Propofol. *Curr Neuropharmacol* **14**: 772-780.
- Franks NP (2015) Structural comparisons of ligand-gated ion channels in open, closed, and desensitized states identify a novel propofol-binding site on mammalian  $\gamma$ -aminobutyric acid type A receptors. *Anesthesiology* **122**: 787-794.
- Germann AL, Pierce SR, Evers AS, Steinbach JH, and Akk G (2022) Perspective on the Relationship between GABAA Receptor Activity and the Apparent Potency of an Inhibitor. *Curr Neuropharmacol* **20**: 90-93.

- Germann AL, Pierce SR, Senneff TC, Burbridge AB, Steinbach JH, and Akk G (2019) Steady-state activation and modulation of the synaptic-type  $\alpha 1\beta 2\gamma 2\text{L}$  GABAA receptor by combinations of physiological and clinical ligands. *Physiol Rep* **7**: e14230.
- Hassan NM, Alhossary AA, Mu Y, and Kwoh CK (2017) Protein-Ligand Blind Docking Using QuickVina-W With Inter-Process Spatio-Temporal Integration. *Sci Rep* **7**: 15451.
- Hines RM, Davies PA, Moss SJ, and Maguire J (2012) Functional regulation of GABAA receptors in nervous system pathologies. *Curr Opin Neurobiol* **22**: 552-558.
- Hoyt H, Fantasia RJ, Bhawe K, Yang X, and Forman SA (2022) Photomotor Responses in Zebrafish and Electrophysiology Reveal Varying Interactions of Anesthetics Targeting Distinct Sites on gamma-Aminobutyric Acid Type A Receptors. *Anesthesiology* **137**: 568-585.
- Huang J, Rauscher S, Nawrocki G, Ran T, Feig M, de Groot BL, Grubmuller H, and MacKerell AD, Jr. (2017) CHARMM36m: an improved force field for folded and intrinsically disordered proteins. *Nat Methods* **14**: 71-73.
- Humphrey W, Dalke A, and Schulten K (1996) VMD: visual molecular dynamics. *J Mol Graph* **14**: 33-38, 27-38.
- Kim JJ, Gharpure A, Teng J, Zhuang Y, Howard RJ, Zhu S, Noviello CM, Walsh RM, Jr., Lindahl E, and Hibbs RE (2020) Shared structural mechanisms of general anaesthetics and benzodiazepines. *Nature* **585**: 303-308.
- Li GD, Chiara DC, Sawyer GW, Husain SS, Olsen RW, and Cohen JB (2006a) Identification of a GABAA receptor anesthetic binding site at subunit interfaces by photolabeling with an etomidate analog. *J Neurosci* **26**: 11599-11605.
- Li P, Covey DF, Steinbach JH, and Akk G (2006b) Dual potentiating and inhibitory actions of a benz[e]indene neurosteroid analog on recombinant  $\alpha 1\beta 2\gamma 2$  GABAA receptors. *Mol Pharmacol* **69**: 2015-2026.

- Michel MC, Murphy TJ, and Motulsky HJ (2020) New Author Guidelines for Displaying Data and Reporting Data Analysis and Statistical Methods in Experimental Biology. *Mol Pharmacol* **97**: 49-60.
- Nourmahnad A, Stern AT, Hotta M, Stewart DS, Ziemba AM, Szabo A, and Forman SA (2016) Tryptophan and cysteine mutations in M1 helices of  $\alpha 1\beta 3\gamma 2\text{L}$  G-aminobutyric acid type A receptors indicate distinct intersubunit sites for four intravenous anesthetics and one orphan site. *Anesthesiology* **125**: 1144-1158.
- Pierce SR, Germann AL, Steinbach JH, and Akk G (2022) The Sulfated Steroids Pregnenolone Sulfate and Dehydroepiandrosterone Sulfate Inhibit the  $\alpha 1\beta 3\gamma 2\text{L}$  GABA(A) Receptor by Stabilizing a Novel Nonconducting State. *Mol Pharmacol* **101**: 68-77.
- Saari TI, Uusi-Oukari M, Ahonen J, and Olkkola KT (2011) Enhancement of GABAergic activity: neuropharmacological effects of benzodiazepines and therapeutic use in anesthesiology. *Pharmacol Rev* **63**: 243-267.
- Sakamoto S, Yamaura K, Numata T, Harada F, Amaike K, Inoue R, Kiyonaka S, and Hamachi I (2019) Construction of a Fluorescent Screening System of Allosteric Modulators for the GABAA Receptor Using a Turn-On Probe. *ACS Cent Sci* **5**: 1541-1553.
- Schrödinger (2020) Schrödinger suite. Schrödinger Release 2020-3.
- Shin DJ, Germann AL, Covey DF, Steinbach JH, and Akk G (2019) Analysis of GABAA receptor activation by combinations of agonists acting at the same or distinct binding sites. *Molecular Pharmacology* **95**: 70-81.
- Shin DJ, Germann AL, Steinbach JH, and Akk G (2017) The actions of drug combinations on the GABAA receptor manifest as curvilinear isoboles of additivity. *Mol Pharmacol* **92**: 556-563.
- Sieghart W and Savic MM (2018) International Union of Basic and Clinical Pharmacology. CVI: GABAA Receptor Subtype- and Function-selective Ligands: Key Issues in Translation to Humans. *Pharmacol Rev* **70**: 836-878.

- Sigel E and Ernst M (2018) The Benzodiazepine Binding Sites of GABAA Receptors. *Trends Pharmacol Sci* **39**: 659-671.
- Steinbach JH and Akk G (2019) Applying the Monod-Wyman-Changeux Allosteric Activation Model to Pseudo-Steady-State Responses from GABAA Receptors. *Mol Pharmacol* **95**: 106-119.
- Szabo A, Nourmahnad A, Halpin E, and Forman SA (2019) Monod-Wyman-Changeux Allosteric Shift Analysis in Mutant  $\alpha 1\beta 3\gamma 2L$  GABAA Receptors Indicates Selectivity and Crosstalk among Intersubunit Transmembrane Anesthetic Sites. *Mol Pharmacol* **95**: 408-417.
- Tang X, Jaenisch R, and Sur M (2021) The role of GABAergic signalling in neurodevelopmental disorders. *Nat Rev Neurosci* **22**: 290-307.
- Wang E, Sun H, Wang J, Wang Z, Liu H, Zhang JZH, and Hou T (2019) End-Point Binding Free Energy Calculation with MM/PBSA and MM/GBSA: Strategies and Applications in Drug Design. *Chem Rev* **119**: 9478-9508.
- Wang M, He Y, Eisenman LN, Fields C, Zeng CM, Mathews J, Benz A, Fu T, Zorumski E, Steinbach JH, Covey DF, Zorumski CF, and Mennerick S (2002)  $3\beta$  -hydroxypregnane steroids are pregnenolone sulfate-like GABA(A) receptor antagonists. *J Neurosci* **22**: 3366-3375.
- Weir CJ, Mitchell SJ, and Lambert JJ (2017) Role of GABAA receptor subtypes in the behavioural effects of intravenous general anaesthetics. *Br J Anaesth* **119**: i167-i175.
- Williams-Noonan BJ, Yuriev E, and Chalmers DK (2018) Free Energy Methods in Drug Design: Prospects of "Alchemical Perturbation" in Medicinal Chemistry. *J Med Chem* **61**: 638-649.
- Wu EL, Cheng X, Jo S, Rui H, Song KC, Davila-Contreras EM, Qi Y, Lee J, Monje-Galvan V, Venable RM, Klauda JB, and Im W (2014) CHARMM-GUI Membrane Builder toward realistic biological membrane simulations. *J Comput Chem* **35**: 1997-2004.

## **Footnotes**

This work was supported by the National Institutes of Health National Institute of General Medical Sciences [Grant GM140947]; IMI2 project NeuroDerisk (821528); Italian Ministry of Instruction, University and Research (MIUR), Italy; the Taylor Family Institute for Innovative Psychiatric Research; and by an OVPR Pilot/Seed Grant (Oklahoma State University Center for Health Sciences). No author has an actual or perceived conflict of interest with the contents of this article.

## Legends for Figures

**Figure 1. Chemical synthesis.** (A) Synthesis of DM497 (a), DM492 (b), DM495 (c), DM480 (d), and PAM-4 (e). The suitable carboxylic acid was reacted with different amines in  $\text{CH}_2\text{Cl}_2$  in the presence of  $\text{Et}_3\text{N}$  and using EDC and HOBt as coupling reagents. The respective amines were: p-toluidine (a), tetrahydroquinoline (b); tetrahydroisoquinoline (c), 1-aminoindoline hydrochloride (d), and aniline (e). (B) Synthesis of DM490. The NH group of PAM-2 was first deprotonated using NaH in THF and then alkylated with MeI (f). More details are provided in Methods.

**Figure 2. Fluorescence measurements.** Confocal images of HEK293T  $\alpha 1\beta 3\gamma 2\text{L}$  cells upon the addition of the turn-on fluorescent probe Gzn-OG (100 nM), in the absence and presence of increasing concentrations (1  $\mu\text{M}$ -10 mM) of GABA, administered alone or in the presence of 100  $\mu\text{M}$  of each DM compound.

**Figure 3. DM compounds modify apparent GABA binding affinity.** (A-F) Fluorescence intensity of HEK293T- $\alpha 1\beta 3\gamma 2\text{L}$ -bound Gzn-OG in the presence over absence ( $F/F_0$ ) of 0.01  $\mu\text{M}$ -30 mM GABA applied alone (●) or in combination with 10 (●), 30 (●) or 100  $\mu\text{M}$  (●) DM497 (A), DM490 (B), DM492 (C), DM495 (D), DM489 (E), and DM480 (F). The data points show mean  $\pm$  S.E.M. from 12 to 22 cells (see below for specifics). The GABA  $\text{IC}_{50}\text{s}$  were estimated from non-linear regression analysis of  $F/F_0$  vs [GABA] relationships. The estimated  $\text{IC}_{50}\text{s}$  for the DM497 dataset are:  $47.5 \pm 4.6 \mu\text{M}$  (GABA alone,  $n = 22$  cells),  $5.0 \pm 0.3 \mu\text{M}$  (10  $\mu\text{M}$  DM497,  $n = 16$ ),  $2.2 \pm 0.2 \mu\text{M}$  (30  $\mu\text{M}$  DM497,  $n = 15$ ), and  $0.6 \pm 0.4 \mu\text{M}$  (100  $\mu\text{M}$  DM497,  $n = 16$ ). The estimated  $\text{IC}_{50}\text{s}$  for the DM490 dataset are:  $46.5 \pm 3.3 \mu\text{M}$  (GABA alone,  $n = 15$ ),  $2.8 \pm 0.2 \mu\text{M}$  (10  $\mu\text{M}$  DM490,  $n = 14$ ),  $2.1 \pm 0.2 \mu\text{M}$  (30  $\mu\text{M}$  DM490,  $n = 14$ ), and  $0.6 \pm 0.1 \mu\text{M}$  (100  $\mu\text{M}$  DM490,  $n = 14$ ). The estimated  $\text{IC}_{50}\text{s}$  for the DM492 dataset are:  $46.5 \pm 3.3 \mu\text{M}$  (GABA alone,  $n = 15$ ),  $9.9 \pm 0.5 \mu\text{M}$  (10  $\mu\text{M}$  DM492,  $n = 15$ ),  $2.9 \pm 0.4 \mu\text{M}$  (30  $\mu\text{M}$  DM492,  $n = 16$ ), and  $0.7 \pm 0.1 \mu\text{M}$  (100  $\mu\text{M}$  DM492,  $n = 18$ ). The estimated  $\text{IC}_{50}\text{s}$  for the DM495 dataset are:  $36.6 \pm 3.2 \mu\text{M}$  (GABA alone,  $n = 20$ ),  $29.3 \pm 3.1 \mu\text{M}$  (10



$\mu\text{M}$  DM495,  $n = 17$ ),  $18.4 \pm 1.6 \mu\text{M}$  ( $30 \mu\text{M}$  DM495,  $n = 15$ ), and  $4.3 \pm 0.3 \mu\text{M}$  ( $100 \mu\text{M}$  DM495,  $n = 15$ ). The estimated  $\text{IC}_{50}\text{s}$  for the DM489 dataset are:  $53.5 \pm 3.2 \mu\text{M}$  (GABA alone,  $n = 16$ ),  $24.8 \pm 2.0 \mu\text{M}$  ( $10 \mu\text{M}$  DM489,  $n = 16$ ),  $10.7 \pm 0.7 \mu\text{M}$  ( $30 \mu\text{M}$  DM489,  $n = 21$ ), and  $5.9 \pm 0.4 \mu\text{M}$  ( $100 \mu\text{M}$  DM489,  $n = 12$ ). The estimated  $\text{IC}_{50}\text{s}$  for the DM480 dataset are:  $36.5 \pm 3.2 \mu\text{M}$  (GABA alone,  $n = 20$ ),  $24.6 \pm 1.7 \mu\text{M}$  ( $10 \mu\text{M}$  DM480,  $n = 20$ ),  $14.9 \pm 0.6 \mu\text{M}$  ( $30 \mu\text{M}$  DM480,  $n = 21$ ), and  $12.9 \pm 1.1 \mu\text{M}$  ( $100 \mu\text{M}$  DM480,  $n = 16$ ). The  $\text{IC}_{50}$  values were transformed to apparent  $\text{K}_{\text{d,GABA}}$  values using Eq. (2), and are provided in Table 2. **(G)** The effects of DM497 and DM490, as representative DM compounds, on  $\alpha 1\beta 3\gamma 2\text{L}$  GABA<sub>A</sub>R-bound Gzn-OG ( $n = 16$  cells for each compound). The DM compounds did not displace Gzn-OG from the orthosteric binding site at concentrations up to  $100 \mu\text{M}$ .

**Figure 4. Electrophysiological activity of novel DM compounds and PAM-4 on the  $\alpha 1\beta 2\gamma 2\text{L}$  GABA<sub>A</sub>R activated by low GABA.** Representative GABA ( $3\text{--}10 \mu\text{M}$ )-induced currents in the absence and presence of DM490 **(A)**, DM497 **(B)**, or DM492 **(C)**. **(D)** Concentration-response relationships for DM490, DM497, and DM492. The data points show mean  $\pm$  S.D. from 5 (DM490 and DM497) or 6 (DM492) oocytes. Each oocyte was exposed to the full range of drug concentrations. The fitted  $\text{EC}_{50}$ ,  $E_{\text{max}}$ , and  $n_{\text{H}}$  values are summarized in Table 3.

**Figure 5. Comparison of the effects of novel DM compounds on  $\alpha 1\beta 3\gamma 2\text{L}$  and  $\alpha 1\beta 2\gamma 2\text{L}$  GABA<sub>A</sub>Rs.** The data show potentiation (mean  $\pm$  SD;  $n = 5\text{--}6$  oocytes) of current responses to low GABA by  $50 \mu\text{M}$  DM490, DM492 and DM495, and  $100 \mu\text{M}$  DM497 and DM489. No statistically significant difference between the two subtypes was observed.

**Figure 6. Inhibitory activity of PAM-4 on the  $\alpha 1\beta 2\gamma 2\text{L}$  GABA<sub>A</sub>R.** **(A)** Representative GABA ( $1 \text{ mM}$ )-induced GABA<sub>A</sub>R currents in the absence and presence of PAM-4. The modulator was coapplied with GABA during the desensitization decay phase of the response to GABA. The traces

are from different cells. **(B)** Representative currents induced by 10  $\mu$ M GABA + 200  $\mu$ M PAM-4 in the absence and presence of DM497. All traces are from the same cell. The dotted line in the first trace gives the level of peak response to 10  $\mu$ M GABA in the absence of modulators in this cell. **(C)** The concentration-response relationships show the inhibitory effect of PAM-4 on currents elicited by 1 mM GABA, and the potentiating effect of DM497 on receptors activated by 10  $\mu$ M GABA in the presence of 200  $\mu$ M PAM-4. The dashed line gives the potentiating effect of DM497 alone (reproduced from Fig. 4D). The fitted  $IC_{50}$  and  $EC_{50}$  values are given in the text.

**Figure 7. Comparison of inhibition and potentiation in  $\alpha 1\beta 2\gamma 2L$  and  $\alpha 1(V256S)\beta 2\gamma 2L$  GABA<sub>A</sub>Rs.** **(A)** Representative GABA<sub>A</sub>R currents elicited by high (1 mM) GABA in the absence and presence of 50  $\mu$ M DM490 or 100  $\mu$ M PAM-4. The inhibitory effects of DM490 and PAM-4 are abolished in the mutant receptor. **(B)** Summary of findings. The  $\alpha 1(V256S)$  mutation abolishes inhibition by all tested compounds (wild-type: black circles, mutant: blue squares). **(C)** Representative GABA<sub>A</sub>R currents elicited by low (1  $\mu$ M in wild-type, 0.05  $\mu$ M in the mutant) in the absence and presence of 50  $\mu$ M DM490 or 200  $\mu$ M PAM-4. The potentiating effect of DM490 is retained in the mutant receptor. The mutation also reveals a small potentiating effect of PAM-4 (bottom right trace). **(D)** Summary of findings. The  $\alpha 1(V256S)$  mutation does not modify potentiation by the DM compounds, but converts the effect of PAM-4 from inhibition to potentiation ( $P < 0.01$  vs. no effect; paired t-test; Excel, Microsoft, Redmond, WA). The data for the wild-type receptor are reproduced from Figure 5.

**Figure 8. Molecular docking of DM490, DM497, and PAM-4 in the  $\alpha 1\beta 2\gamma 2L$  GABA<sub>A</sub>R model.** **(A)** Stable docking sites for DM490 (red) at the  $\beta +/\alpha -$  and  $\alpha +/\beta -$  interfaces (left panel), DM497 (yellow) at the  $\gamma +/\beta -$  and  $\alpha +/\gamma -$  interfaces (middle panel), and PAM-4 (blue) in the ion channel (right panel). Subunits ( $\alpha$ , white;  $\beta$ , light-blue; and  $\gamma$ , red) are represented as ribbons, while ligands are represented as molecular surfaces. **(B)** RMSD plots for the 100-ns MD simulations for DM490,

DM497, and PAM-4 at each intersubunit site and at the ion channel site. ( $\alpha^+$ ) $\beta^+/\alpha^-$  (●●●●), ( $\gamma^+$ ) $\beta^+/\alpha^-$  (---),  $\alpha^+/\beta^-$  (●●●●),  $\gamma^+/\beta^-$  (----),  $\alpha^+/\gamma^-$  (-----), and ion channel lumen (-----).

**Figure 9. Molecular interactions of DM490, DM497, and PAM-4 in the  $\alpha 1\beta 2\gamma 2L$  GABA<sub>A</sub>R model.** DM490 at the  $\beta^+/\alpha^-$  (A) and  $\alpha^+/\beta^-$  (B) sites, and DM497 at the  $\gamma^+/\beta^-$  (C) and  $\alpha^+/\gamma^-$  (D) sites. (E) Molecular interactions for PAM-4 at the ion channel site. The ligands are represented as thin sticks, colored by atoms, with carbon atoms in green, while the interacting residues are represented by thick sticks, colored by atoms, where H atoms are omitted for clarity. Red dotted lines represent  $\pi$ - $\pi$  interactions. The involved residues at each site are summarized in Table 5.

**Figure 10. Effects of allosteric agonists and mutations on potentiation by DM490.** (A-B) Comparison of DM490-induced potentiation of  $\alpha 1\beta 2\gamma 2L$  receptors activated by low concentrations of etomidate (Eto, 7-10  $\mu$ M), phenobarbital (PhB, 0.75-1 mM), or GABA (0.5-1  $\mu$ M). DM490 was applied at 50  $\mu$ M. The current trace and summary data for GABA are reproduced from Figures 5 and 7. Statistical significance between the effects of DM490 on receptors activated by GABA, etomidate, or phenobarbital was determined using one-way ANOVA ( $F(2,16) = 54.65$ ,  $P < 0.001$ ) followed by Dunnett's post-hoc multiple comparisons test (Stata/IC 12.1, StataCorp, College Station, TX, USA). \* indicates significance at  $P < 0.01$ . (C) Effects of mutations on receptor potentiation or activation by 50  $\mu$ M DM490. The  $\alpha 1\beta 2(F289A)\gamma 2L$  and  $\alpha 1(Y293C)\beta 2\gamma 2L$  receptors were activated by low concentrations of GABA (0.1-0.2  $\mu$ M) in the absence and presence of 50  $\mu$ M DM490. The  $\alpha 1\beta 2\gamma 2L(L246W)$  and  $\alpha 1\beta 2\gamma 2L(F304C)$  receptors were constitutively active, shown by upward deflection of current upon the application of 200  $\mu$ M picrotoxin (PTX). The effect of DM490 on the holding current in  $\alpha 1\beta 2\gamma 2L(L246W)$  and  $\alpha 1\beta 2\gamma 2L(F304C)$  receptors was measured by comparing the direct activating response to DM490, the inhibitory effect of picrotoxin, and the activating effect of 1 mM GABA + 50  $\mu$ M propofol in the same cell. (D) The column graph summarizes DM490 effects on the  $\alpha 1\beta 2(F289A)\gamma 2L$  ( $\beta^+/\alpha^-$  interface with the mutation in the  $\beta$  subunit),

$\alpha 1(Y293C)\beta 2\gamma 2L$  ( $\alpha^{+}/\beta^{-}$  and  $\alpha^{+}/\gamma^{-}$  interfaces with the mutation in the  $\alpha$  subunit),  $\alpha 1\beta 2\gamma 2L(L246W)$  ( $\alpha^{+}/\gamma^{-}$  interface with the mutation in the  $\gamma$  subunit), and  $\alpha 1\beta 2\gamma 2L(F304C)$  ( $\gamma^{+}/\beta^{-}$  interface with the mutation in the  $\gamma$  subunit) receptors. The thick and thin dotted lines indicate mean  $\pm$  1 S.D. potentiation in the  $\alpha 1\beta 2\gamma 2L$  receptor. Statistical significance between the effects of DM490 on  $\alpha 1\beta 2\gamma 2L$  and the mutant receptors was determined by one-way ANOVA ( $F(4,21) = 83.00$ ,  $P < 0.001$ ) followed by Dunnett's post-hoc multiple comparisons test (\*,  $P < 0.01$ ; ns,  $P > 0.05$ ).

**Figure 11. Effects of an allosteric inhibitor and mutations on inhibition by PAM-4.** (A) Representative GABA<sub>A</sub>R current elicited by 1 mM GABA in the absence and presence of 10  $\mu$ M PS and PS + 200  $\mu$ M PAM-4 in the  $\alpha 1\beta 2\gamma 2L$  receptor. Exposure to PS reduces steady-state current. Coapplication of PAM-4 enhances PS-induced inhibition. The inset shows the effects of PS and PAM-4 at higher ordinate resolution. (B) Comparison of the effects of 200  $\mu$ M PAM-4 and 10  $\mu$ M PS on current elicited by 1 mM GABA in the  $\alpha 1\beta 2\gamma 2L(L274C)$  receptor. The receptor is constitutively active as shown by apparent outward current upon exposure to 200  $\mu$ M picrotoxin (PTX). (C) Comparison of the effects of 200  $\mu$ M PAM-4 and 10  $\mu$ M PS on current elicited by 1 mM GABA in the  $\alpha 1\beta 2\gamma 2L(T278C)$  receptor. Picrotoxin had minimal effect on holding current indicating low constitutive activity. (D) Summary of the effects of 200  $\mu$ M PAM-4 and 10  $\mu$ M PS on the  $\alpha 1\beta 2\gamma 2L(L274C)$ ,  $\alpha 1\beta 2\gamma 2L(T278C)$ , and  $\alpha 1\beta 2\gamma 2L$  receptors. Statistical significance between the effects of PAM-4 on the wild-type and mutant receptors was determined using one-way ANOVA ( $F(2,12) = 35.55$ ,  $P < 0.001$ ) followed by Dunnett's post-hoc multiple comparisons test (Stata/IC 12.1, StataCorp, College Station, TX, USA). \* indicates significance at  $P < 0.01$ .

**Table 1.** Molecular descriptors for the DM compounds, PAM-4 and PAM-2.

Compound	MolVol (Å <sup>3</sup> )	H donor/acceptor	LogP	LogBB
DM497	193	1/1	3.52	0.39
DM490	199	0/1	3.17	0.30
DM480	200	1/2	2.78	-0.06
DM492	204	0/1	3.21	0.31
DM495	212	0/1	3.22	0.32
DM489 <sup>a</sup>	185	0/1	2.76	0.17
PAM-4 <sup>a</sup>	168	1/1	2.48	-0.06
PAM-2 <sup>a</sup>	182	1/1	2.96	0.09

The table gives the molecular volume (MolVol), hydrogen-bonding capability (H donor/acceptor), and measures of lipophilicity (LogP) and ability to penetrate the blood-brain barrier (LogBB) for the tested DM compounds. All parameters were calculated using the Biovia Discovery Studio software (Dassault Systèmes Co., MA, USA). High LogP indicates high lipophilicity. LogBB values between 0 and 0.7 and between -0.01 and -0.52 indicate high and medium penetration, respectively. <sup>a</sup> The LogP and LogBB values for DM489 and PAM-2 (Arias et al., 2020) and PAM-4 (Bagdas et al., 2021) are included for reference.

**Table 2.** Pharmacological effects of the novel DM compounds on apparent affinity to GABA in the  $\alpha 1\beta 3\gamma 2L$  GABA<sub>A</sub>R.

Compound	$K_{d,GABA}$ (number of cells), $\mu M$	$K_{d,GABA (DM)}$ (number of cells), $\mu M$	$K_{d,GABA}/K_{d,GABA (DM)}$ (fold difference)
DM497	$16.8 \pm 1.6$ (22)	$0.2 \pm 0.2$ (16)	84
DM490	$16.5 \pm 1.2$ (15)	$0.2 \pm 0.02$ (14)	75
DM492	$16.5 \pm 1.2$ (15)	$0.3 \pm 0.03$ (18)	63
DM489	$19.0 \pm 1.1$ (16)	$2.1 \pm 0.2$ (12)	9.1
DM495	$13.0 \pm 1.1$ (20)	$1.5 \pm 0.1$ (15)	8.4
DM480	$13.0 \pm 1.1$ (20)	$4.6 \pm 0.4$ (16)	2.9

$K_{d,GABA}$  and  $K_{d,GABA (DM)}$  reflect the apparent binding affinities to GABA in the absence or presence of 100  $\mu M$  of each tested DM compound. The table gives means  $\pm$  propagated errors (numbers of cells) for  $K_{d,GABA}$  and  $K_{d,GABA (DM)}$  calculated using Eq. (2).

**Table 3.** GABAergic properties of the novel DM compounds and PAM-4.

Compound	EC <sub>50</sub> or IC <sub>50</sub> , $\mu\text{M}$	n <sub>H</sub>	Apparent efficacy, % of control (n cells)	K <sub>R</sub> , $\mu\text{M}$	c <sup>c</sup>	$\Delta\text{G}$ , kcal/mol <sup>f</sup>	Inhibition, % of control (n cells) <sup>g</sup>
DM490	12 [10 to 15] <sup>a</sup>	1.3 $\pm$ 0.2	519 $\pm$ 260 <sup>c</sup> (5)	22 $\pm$ 3	0.22 $\pm$ 0.05	-1.79 $\pm$ 0.28	64 $\pm$ 20 (5)
DM497	32 [20 to 50] <sup>a</sup>	1.5 $\pm$ 0.3	540 $\pm$ 523 <sup>c</sup> (5)	50 $\pm$ 33	0.39 $\pm$ 0.16	-1.23 $\pm$ 0.67	60 $\pm$ 15 (5)
DM492	15 [11 to 19] <sup>a</sup>	2.1 $\pm$ 0.7	398 $\pm$ 165 <sup>c</sup> (6)	19 $\pm$ 7	0.41 $\pm$ 0.16	-1.13 $\pm$ 0.45	55 $\pm$ 12 (5)
DM489	ND	ND	144 $\pm$ 9 <sup>d</sup> (5)	ND	0.83 $\pm$ 0.03	-0.23 $\pm$ 0.04	67 $\pm$ 7 (5)
DM495	ND	ND	189 $\pm$ 53 <sup>d</sup> (5)	ND	0.79 $\pm$ 0.14	-0.30 $\pm$ 0.21	54 $\pm$ 15 (5)
PAM-4	54 $\pm$ 7 <sup>b</sup>	-6.4 $\pm$ 9.2	50 $\pm$ 4 <sup>c</sup> (5-11)	ND	ND	ND	81 $\pm$ 7 (6)

<sup>a</sup> Experiments were performed at low [GABA] (<EC<sub>5-15</sub>; P<sub>A</sub><0.2) (Fig. 3). EC<sub>50</sub>s are given as geometric means [95% confidence intervals].

<sup>b</sup> The IC<sub>50</sub> for PAM-4 was estimated from pooled data using the Hill equation. The numbers of cells were: 5 at 1  $\mu\text{M}$ , 7 at 10  $\mu\text{M}$ , 5 at 50  $\mu\text{M}$ , 5 at 100  $\mu\text{M}$ , 11 at 200  $\mu\text{M}$ , and 7 at 500  $\mu\text{M}$  PAM-4. The IC<sub>50</sub> is given as best-fit parameter  $\pm$  standard error of the fit.

<sup>c</sup> Apparent efficacy is calculated as the ratio of Hill-fitted Y<sub>max</sub> to the peak response to GABA alone, expressed in % of control (100% = no effect).

<sup>d</sup> Estimated at 50  $\mu\text{M}$  concentration of the compound.

<sup>e</sup> c is a measure of efficacy, estimated from fitting a potentiation concentration-response relationship to Eq. (3). For DM489 and DM495, the value of c was calculated from  $P_{A,50 \mu\text{M DM489 or 495}} = 1/(1 + L \times c_{50 \mu\text{M DM489 or 495}}^2)$ .

<sup>f</sup>  $\Delta G$  was calculated as  $NRT \times \ln(c)$ , with the number of binding sites (N) constrained to 2.

<sup>g</sup> Inhibition was measured during a steady-state response to 1 mM GABA, and shows the response remaining following exposure to GABA + 50  $\mu$ M modulator.

ND, not determined.



**Table 4.** Molecular docking and stability of DM490, DM497, and PAM-4 at different subunit interfaces and the ion channel of the  $\alpha 1\beta 2\gamma 2$  GABA<sub>A</sub>R model.

Docking site	DM490		DM497		PAM-4	
	TBE (kcal/mol)	RMSD (VAR)	TBE (kcal/mol)	RMSD (VAR)	TBE (kcal/mol)	RMSD (VAR)
$\beta +/\alpha -$ (anesthetic)*	-42	2.9 (0.1)	-43	7.1 (0.1)	-36	3.9 (0.2)
$\alpha +/\beta -$ (anesthetic)	-38	5.1 (0.1)	-38	11.3 (1.0)	-38	13.9 (1.0)
$\gamma +/\beta -$ (anesthetic)	-35	5.7 (1.6)	-39	4.9 (0.1)	-32	12.4 (0.8)
$\alpha +/\gamma -$ (orphan)	-41	17.5 (16.3)	-40	8.0 (0.1)	-29	4.1 (0.9)
Ion channel	-40	3.7 (0.4)	-34	11.1 (2.9)	-27	5.2 (0.1)

TBE: Theoretical binding energy (kcal/mol). More negative values indicate higher binding affinity. Depending on the RMSD VAR values, measured during the last third of the MDs, the observed interactions were considered stable (RMSD VAR <0.2), nearly stable (RMSD VAR 0.2-2), and unstable (RMSD VAR >2).

\*Stable interaction within the  $(\gamma +)\beta +/\alpha -$  interface.

**Table 5.** Molecular interactions of DM490, DM497, and PAM-4 at the subunit interfaces and ion channel of the  $\alpha 1\beta 2\gamma 2$  GABA<sub>A</sub>R model.

Docking Site	DM490		DM497		PAM-4	
Intersubunit Sites						
	(+) side	(−) side	(+) side	(−) side	(+) side	(−) side
β/α (A)	TM2: M261 T262 N265 TM3: L285 M286 <b>F289</b> V290	TM1: I228 Q229 L232 P233 M236	TM2: T262 N265 TM3: D282 L285 M286 F289 V290	TM1: I228 Q229 L232 P233 M236	TM2: M261 T262 N265 TM3: L285 M286 F289 V290	TM1: I228 N229 L232 P233 M236
α/β (A)	TM2: T267 S270 TM3:A283 D287 W288 I290 A291 <b>Y294</b>	TM1: L223 M227 P228 L231	Near stable		Near stable	
γ/β (A)	Near stable		TM2: T277 S280 TM3: S301 <b>F304</b> I305 F308	TM1: L223 Q224 M227 P228 L231	Near stable	
α/γ (O)	Unstable		TM2: S270 TM3: D287 I290 A291 Y294 A295 F298 S299 I302	TM1: I238 I242 L246	Near stable	
Ion Channel Site						
γ subunit	Not found		Not found		TM2: L274 (9'), T277, T278 (13')	
β subunit	Near stable		Unstable		TM1: I232 TM2: I255, T256, L259 (9'), T260, T263 (13'), I264	
α subunit					TM2: T261 (6'), T265	

The "+" and "-" sides indicate contributions made by the two sides of an intersubunit interface within a counter-clockwise order of subunits.

Residues in **bold**:  $\pi$ - $\pi$  interactions. A: Anesthetic site; O: Orphan site.

Residues at 6', 9', and 13' correspond to the canonical TM2 rings in the ion channel lumen.

Figure 1

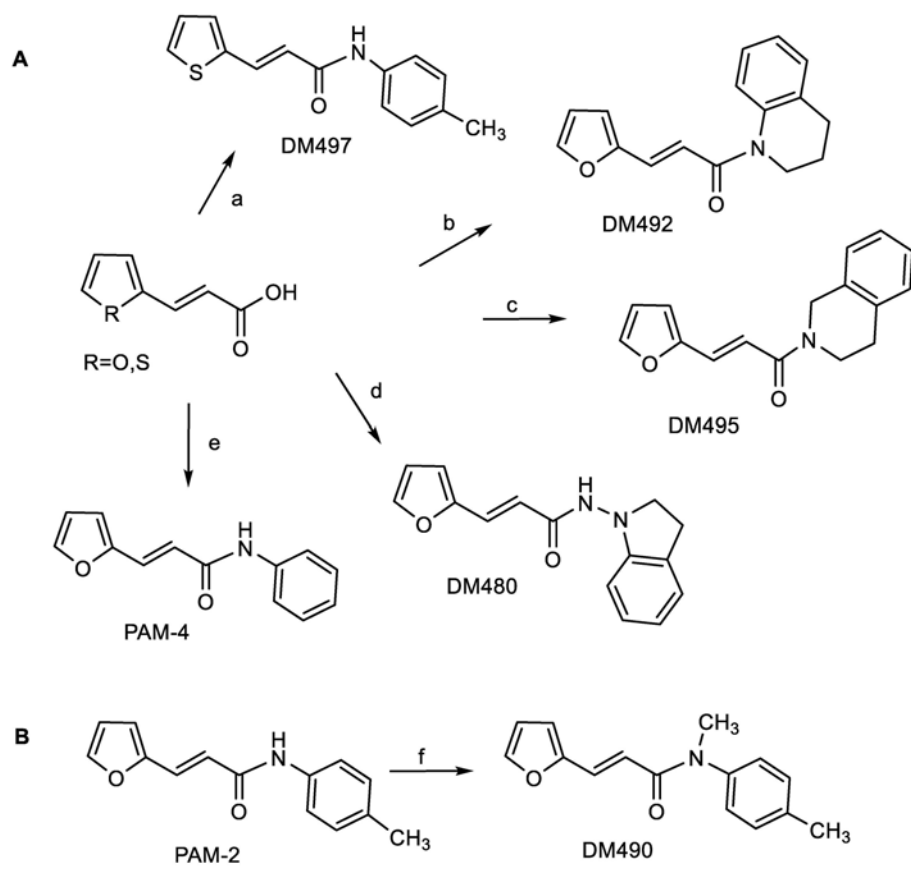


Figure 2

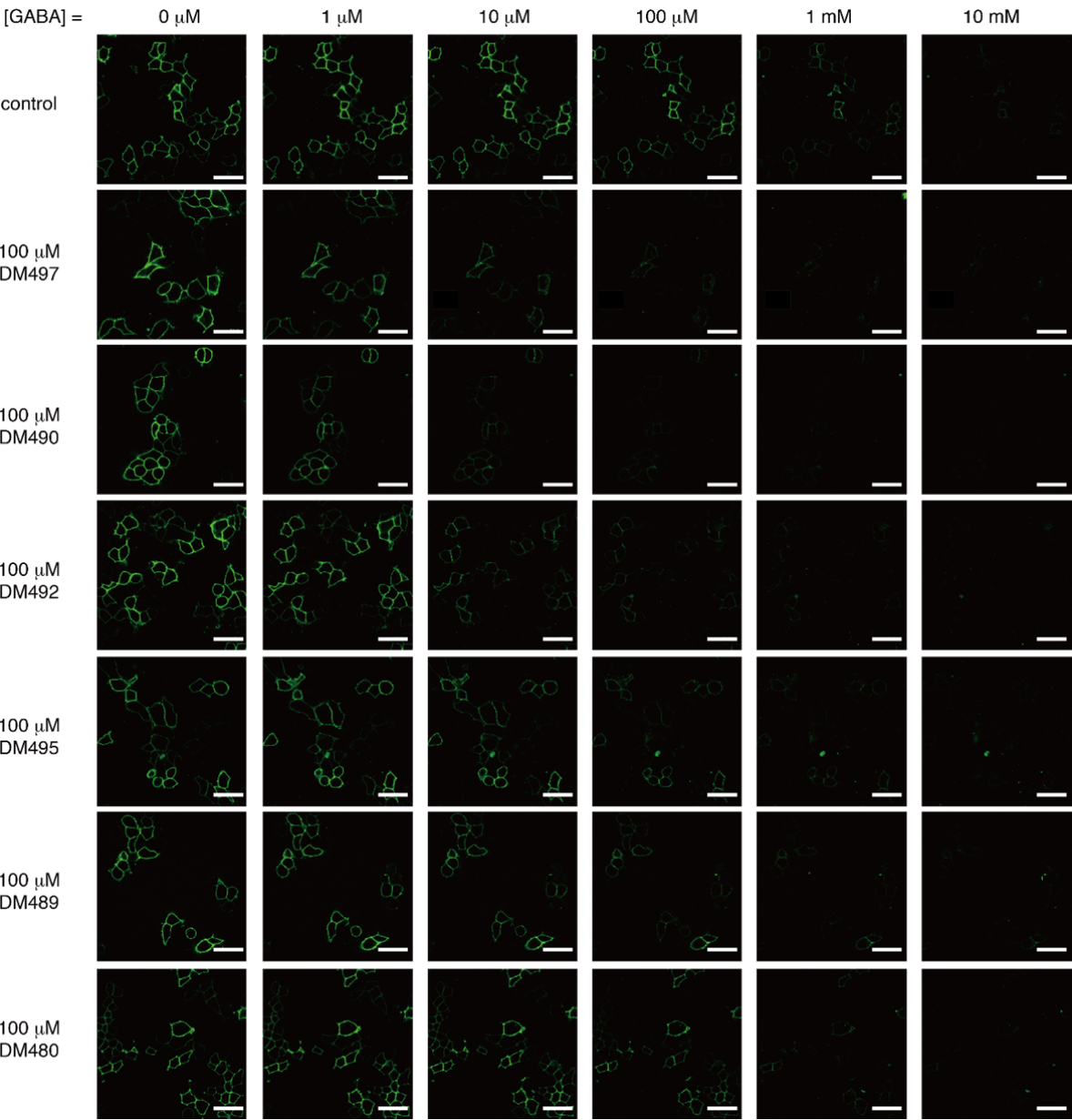


Figure 3

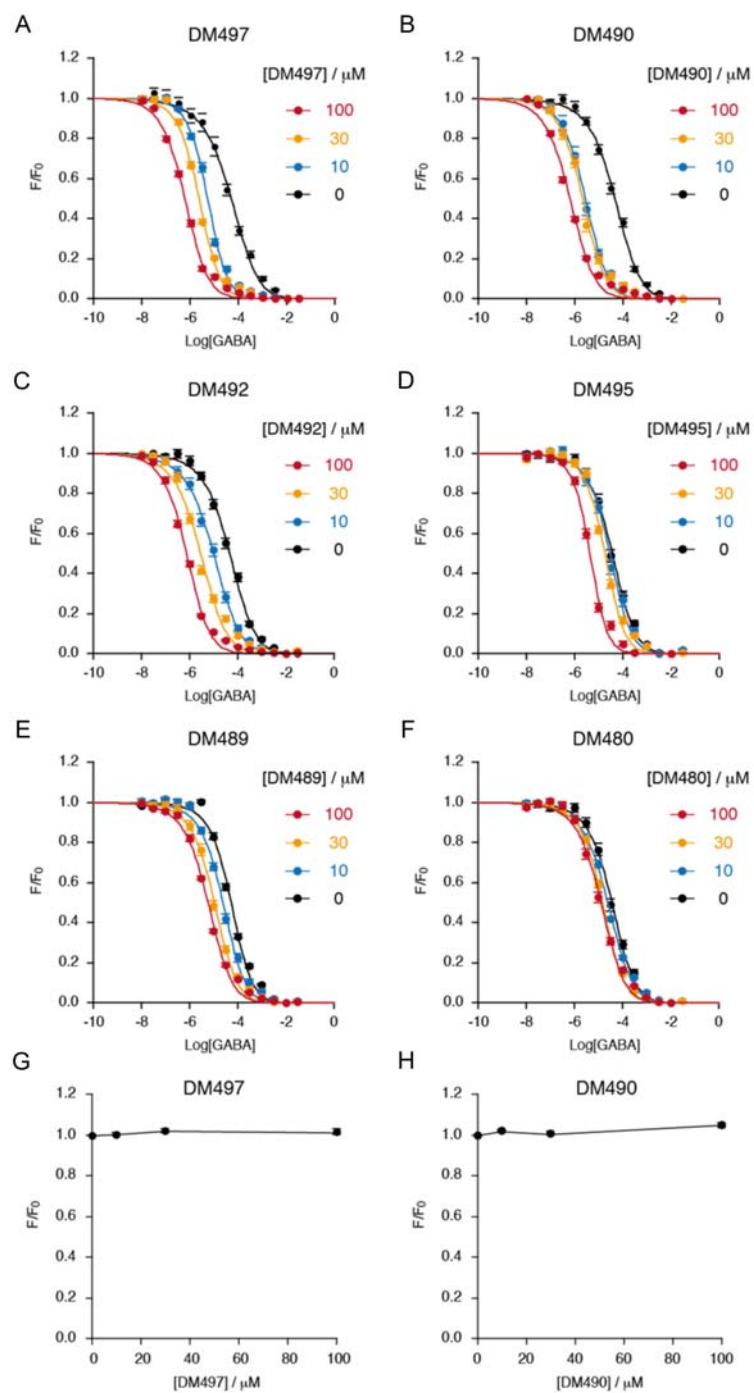


Figure 4

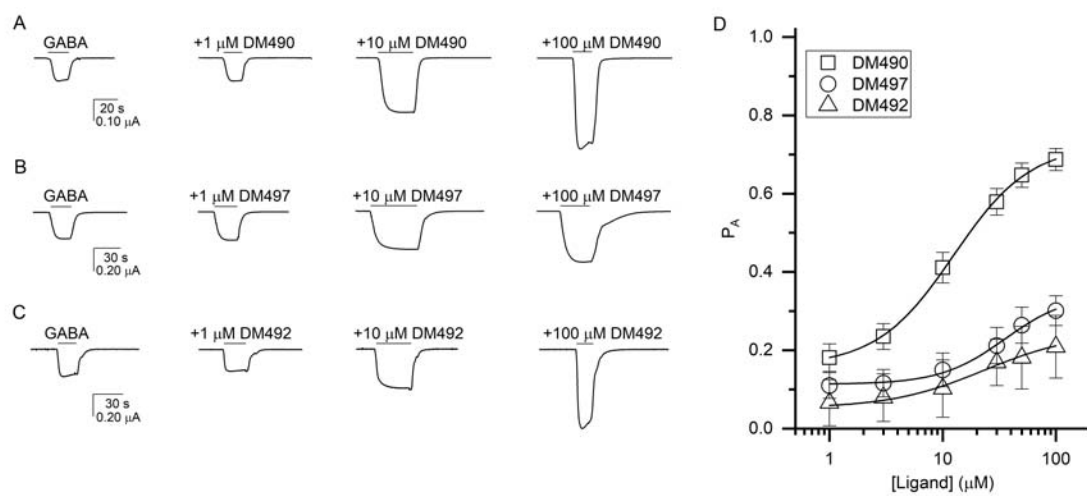


Figure 5

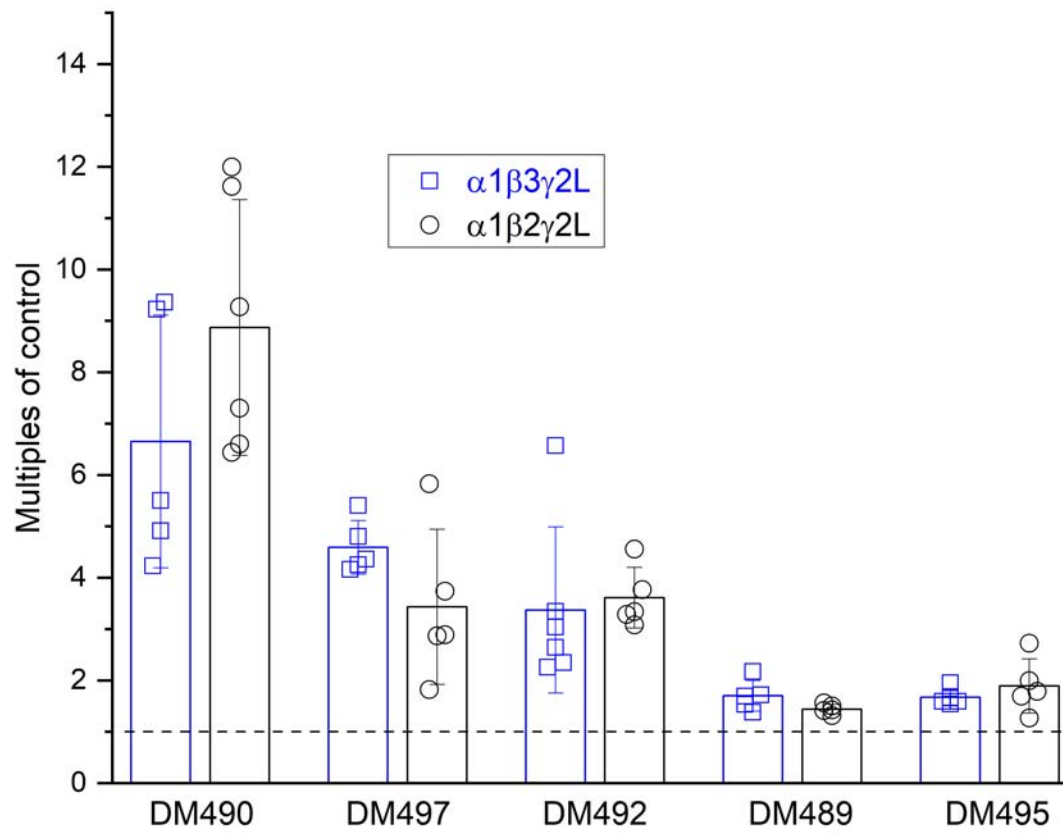


Figure 6

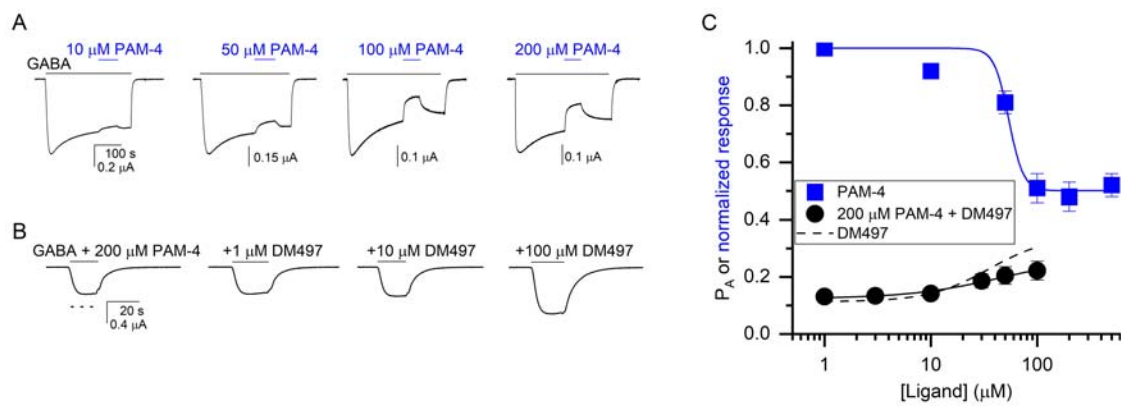




Figure 7

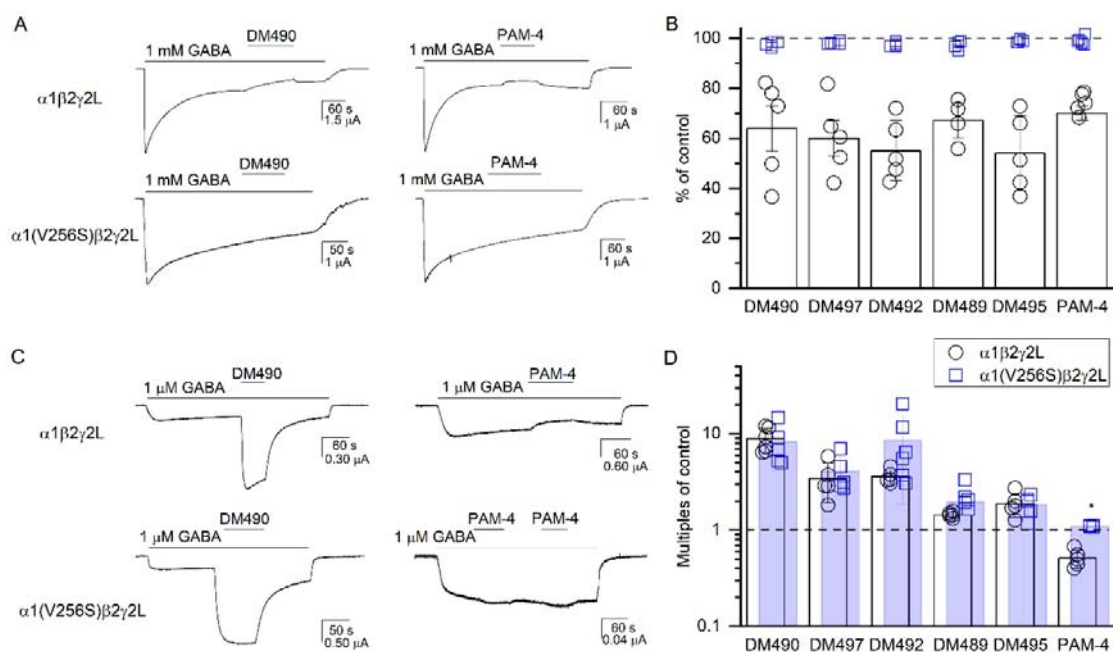


Figure 8

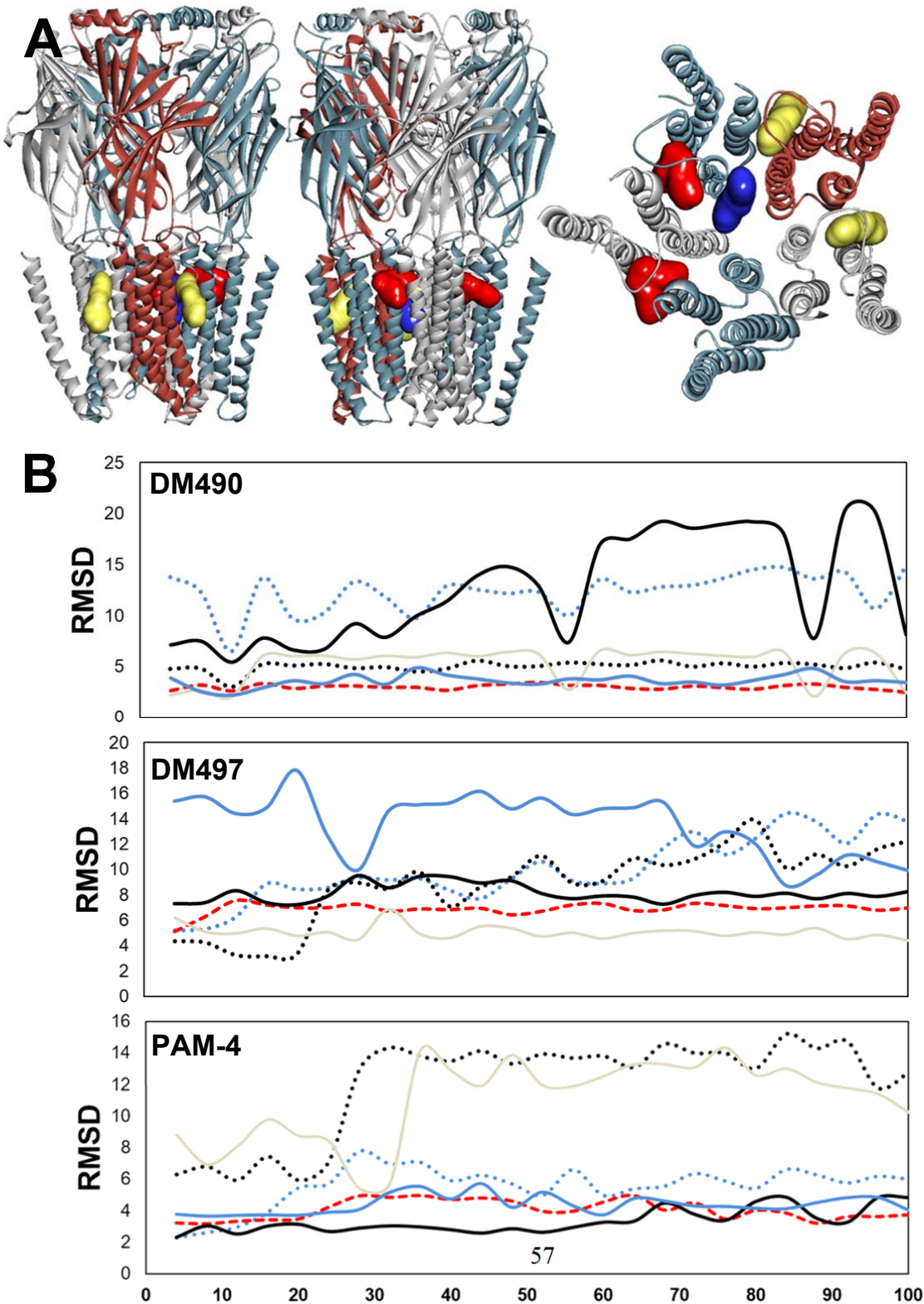


Figure 9

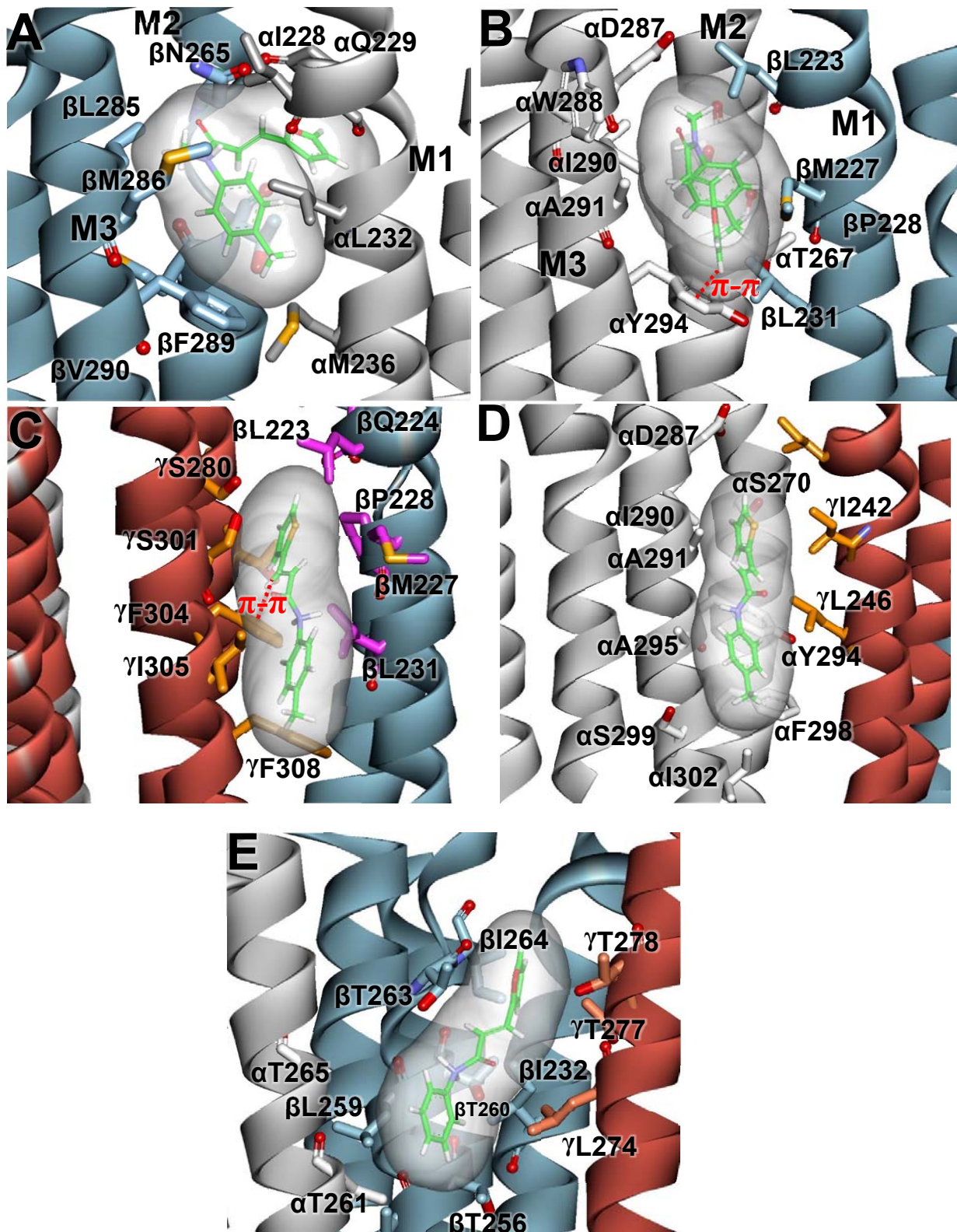


Figure 10

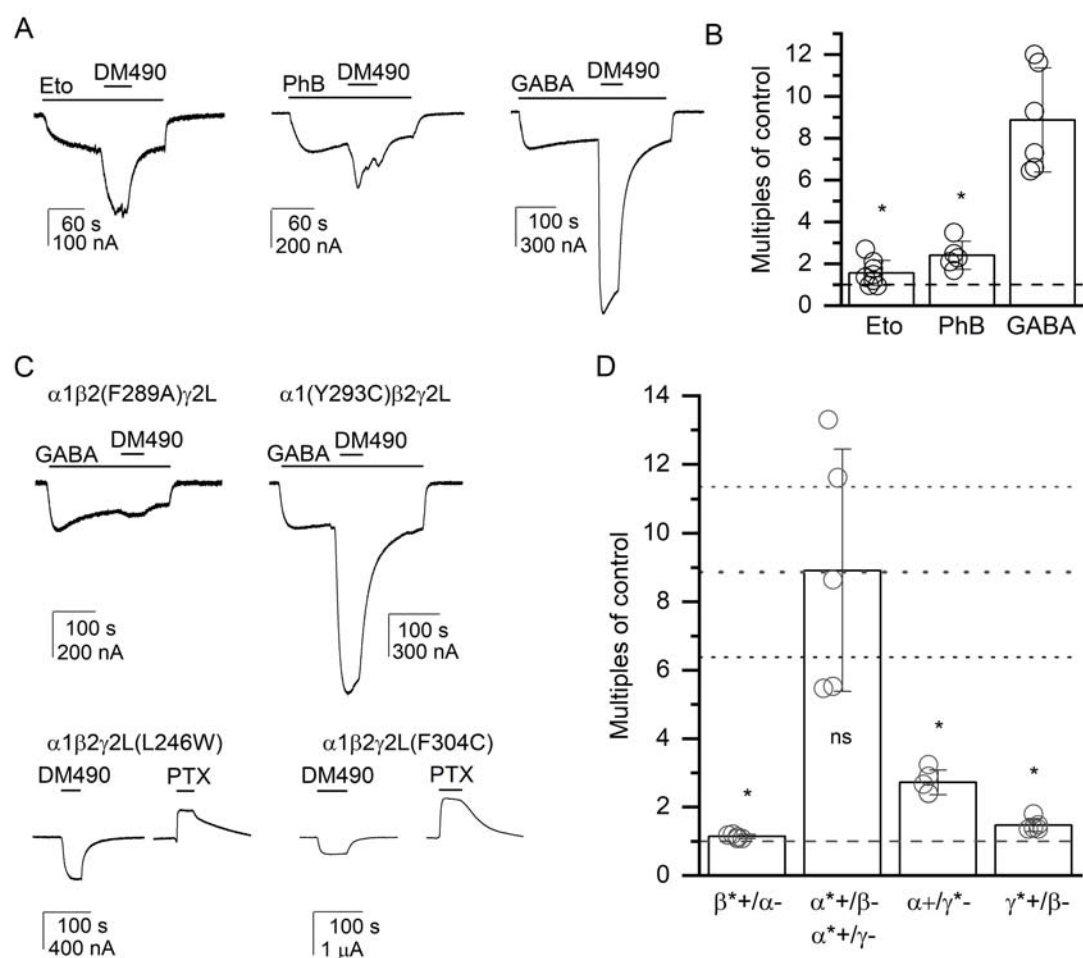
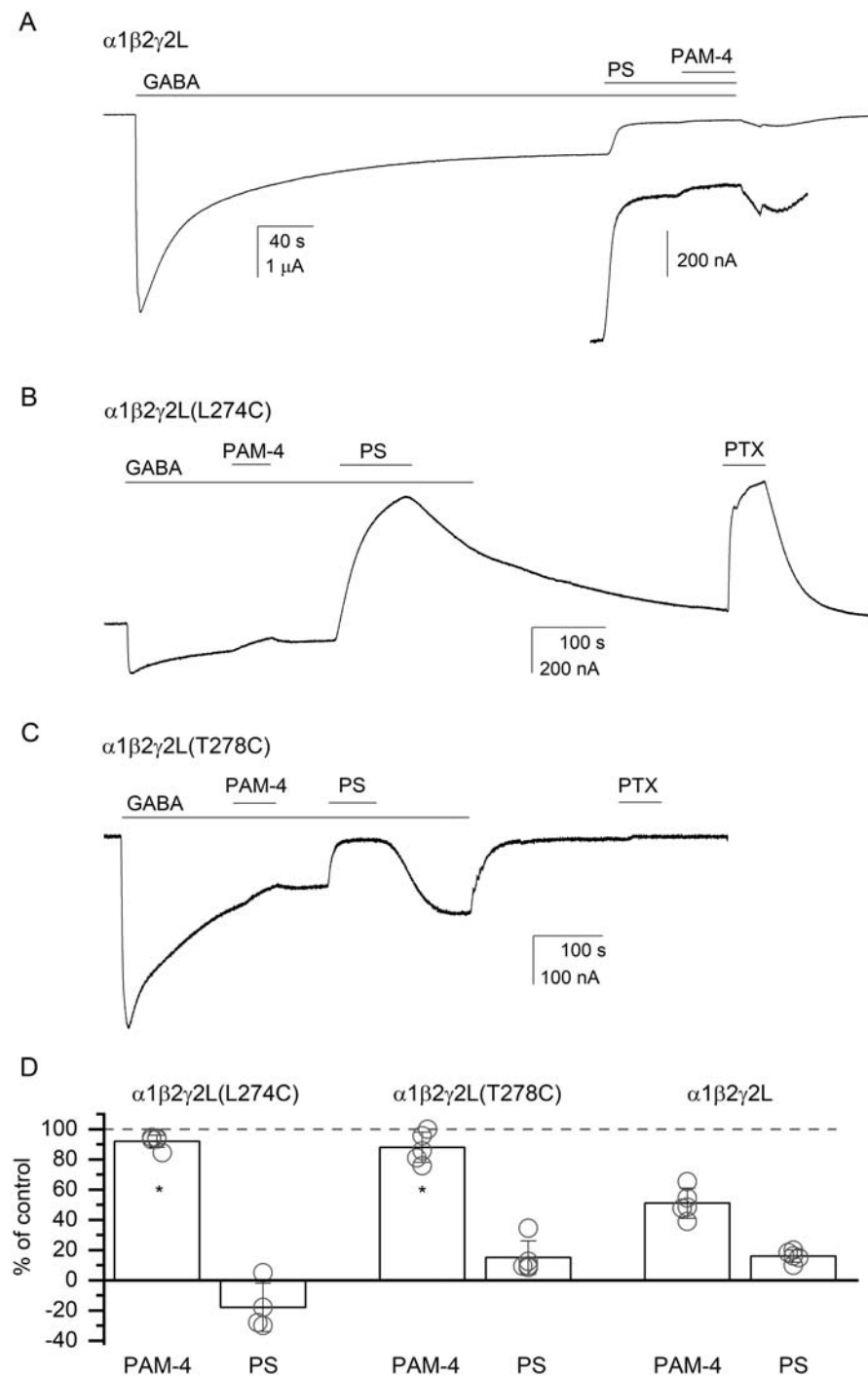


Figure 11



.